HHS Public Access

Author manuscript

Circ Res. Author manuscript; available in PMC 2024 March 03.

Published in final edited form as:

Circ Res. 2023 March 03; 132(5): 545–564. doi:10.1161/CIRCRESAHA.121.320541.

Dysregulated Smooth Muscle Cell BMPR2 – ARRB2 Axis Causes Pulmonary Hypertension

Lingli Wang, MD[1,2,3,4], **Jan Renier Moonen, MD, PhD**[1,2,3,4], **Aiqin Cao, PhD**[1,2,3,4], **Sarasa Isobe, MD**[1,2,3,4], **Caiyun G Li, PhD**[2,3,4], **Nancy F Tojais, PhD**[2,4], **Shalina Taylor, PhD**[2,3,4], **David P Marciano, PhD**[3,5], **Pin-I Chen, PhD**[2,3,4], **Mingxia Gu, MD, PhD**[2,3,4], **Dan Li, PhD**[2,3,4], **Rebecca L Harper, PhD**[2,3,4], **Nesrine El-Bizri, PhD**[2,4], **YuMee Kim, PhD**[2,4], **Kryn Stankunas, PhD**[6], **Marlene Rabinovitch, MD**[1,2,3,4,*]

[1]BASE Initiative, Betty Irene Moore Children's Heart Center, Lucile Packard Children's Hospital

[2]Vera Moulton Wall Center for Pulmonary Vascular Diseases, Stanford University School of Medicine, Stanford, CA, USA

[3]Stanford Cardiovascular Institute, Stanford University School of Medicine, Stanford, CA, USA

[4]Department of Pediatrics (Cardiology), Stanford University School of Medicine, Stanford, CA, USA

[5]Department of Genetics, Stanford University School of Medicine, Stanford, CA, USA

[6]Departments of Pathology and of Developmental Biology, and Howard Hughes Medical Institute; Stanford University School of Medicine, Stanford, CA, USA

Abstract

Rationale: Mutations in bone morphogenetic protein receptor 2 (*BMPR2*) are associated with familial and sporadic pulmonary arterial hypertension (PAH). The functional and molecular link between loss of BMPR2 in pulmonary artery (PA) smooth muscle cells (SMC) and PAH

[*]Corresponding Author: Marlene Rabinovitch, MD, CCSR 1215A, 269 Campus Drive, Stanford University School of Medicine, Stanford, CA 94305-5162, marlener@stanford.edu Phone: 650-723-8239 Fax: 650-723-6700.

Authors' Contributions

L.W. designed and performed the experiments, analyzed and interpreted data, wrote the manuscript, and prepared the figures. J.R.M. performed immunofluorescent staining, acquired confocal images of the human and mouse lung sections, and participated in the data collection and analysis. A.C. performed some RT-qPCR and assisted with the siRNA knockdown. C.G.L. assisted with experimental design, active RHOA and RAC1 pull down assays, and helped with the data collection and analysis. S.I performed the DNA damage *in vitro* experiment, assisted with RVSP measurements, and with the processing of mouse lung tissues. S.T. and D.M. provided valuable guidance and advice and helped with the data collection and analysis. N.T. assisted with confocal microscopy and confocal image analysis of F-Actin in human PASMC. N.E-B. designed and derived the Bmpr2-floxed transgenic mice. Y.K. assisted with RVSP measurements, and with the processing of mouse lung tissues. P.C., R.H., M.G., and D.L. helped with data analysis. K.S. helped in phenotyping the cardiac defect. M.R. designed the studies, and oversaw data acquisition and analysis, and manuscript preparation and editing.

Disclosures: None

Supplemental Materials

Expanded Methods

Online Tables S1 – S2

Online Figures S1 – S9

References 56, 57

Major Resources Table

pathogenesis warrants further investigation, as most investigations focus on BMPR2 in PA endothelial cells.

Objective: Determine whether and how decreased BMPR2 is related to the abnormal phenotype of PASMC in PAH.

Methods: SMC-specific *Bmpr2*$^{-/-}$ mice (*BKO*^{SMC}) were created and compared to controls in room air, after three weeks of hypoxia as a 'second hit', and following four weeks of normoxic recovery. Echocardiography, right ventricular systolic pressure and right ventricular hypertrophy were assessed as indices of pulmonary hypertension (PH). Proliferation, contractility, gene and protein expression of PASMC from *BKO*^{SMC} mice, human PASMC with *BMPR2* reduced by siRNA, and PASMC from PAH patients with a *BMPR2* mutation were compared to controls, to investigate the phenotype and underlying mechanism.

Results: *BKO*^{SMC} mice showed reduced hypoxia-induced vasoconstriction and persistent PH following recovery from hypoxia, associated with sustained muscularization of distal PA. PASMC from mutant compared to control mice displayed reduced contractility at baseline and in response to angiotensin II, increased proliferation and apoptosis resistance. Human PASMC with reduced BMPR2 by siRNA, and PASMC from PAH patients with a *BMPR2* mutation showed a similar phenotype related to upregulation of pERK1/2-pP38-pSMAD2/3 mediating elevation in β-Arrestin2 (ARRB2), pAKT and β-catenin (CTNNB1) and reduction in RHOA and RAC1. Decreasing ARRB2 in PASMC with reduced BMPR2 restored normal signaling, reversed impaired contractility and attenuated heightened proliferation and in mice with inducible loss of BMPR2 in SMC, decreasing ARRB2 prevented persistent PH.

Conclusions: Agents that neutralize the elevated ARRB2 resulting from loss of BMPR2 in PASMC could prevent or reverse the aberrant hypo-contractile and hyperproliferative phenotype of these cells in PAH.

Graphical Abstract

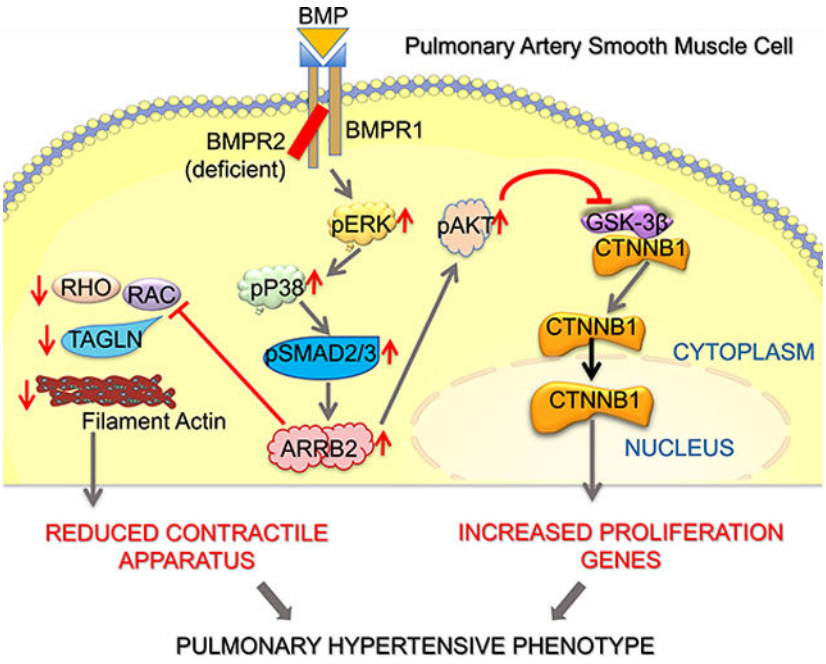

Keywords

Animal Models of Human Disease; Cell Signaling/Signal Transduction; Smooth Muscle Proliferation and Differentiation; Pulmonary Hypertension; Vascular Biology; pulmonary arterial hypertension; smooth muscle cells; BMPR2; β-arrestin2; transgenic mice

Introduction

Despite current vasodilator therapy, pulmonary arterial hypertension (PAH) is frequently a progressive and debilitating disease that is lethal in the absence of a lung transplant. It is characterized by endothelial apoptosis, endothelial to mesenchymal transition with resistance to apoptosis, inflammation, elastic fiber degradation and other changes in the extracellular matrix that contribute to proliferation of vascular smooth muscle-like cells. This culminates in the occlusion and loss of small arteries in the lung, causing severe elevation in pulmonary vascular resistance and right heart failure[1].

Mutations in bone morphogenetic receptor 2 (*BMPR2*) are present in 70% of patients with familial PAH and in 20% of individuals with sporadic idiopathic PAH (IPAH)[2,3], collectively denoted hereditary PAH. Other mutations are infrequent and some impact the BMPR2 signaling pathway, such as those in the co-receptor, activin like kinase-1 gene *(ALK1),* an interacting protein, caveolin-1 gene *(CAV1),* and a downstream transcription factor, mothers against decapentaplegic homolog 9 gene *(SMAD9)*[4]. Notably, BMPR2 expression is reduced in patients with IPAH without an identified mutation, as well as in those whose PAH is associated with other conditions[5]. Numerous investigations have focused on mechanisms relating loss of BMPR2 to pulmonary arterial endothelial cell (PAEC) dysfunction. For example, our group showed that loss of BMPR2 in PAEC causes impaired peroxisome proliferator activated receptor gamma and β-catenin (PPARG-

CTNNB1) dependent angiogenesis[6], associated with a reduction in apelin, a factor that attenuates smooth muscle cell (SMC) proliferation and is anti-inflammatory[7]. More recent studies related loss of BMPR2 to endothelial mesenchymal transition[8] owing to an increase in the chromatin remodeling factor high mobility group AT-hook1 (HMGA1), and in co-culture studies, loss of BMPR2 in PAEC in concert with loss of BMPR2 in pulmonary arterial SMC (PASMC) reduces EC regeneration in response to injury by adversely impacting NOTCH1 signaling[9].

While BMPR2 expression is considerably lower in PASMC compared to PAEC in normal cells, there is substantial evidence that the hyper-proliferative phenotype of PASMC in PAH is also related to a cell autonomous reduction in BMPR2[10] and hence can contribute to lesion formation and progressive obliteration of the pulmonary circulation. Similar to PAH PAEC[6,11–13], PAH PASMC exhibit DNA damage[14], abnormal glycolytic metabolism[15], impaired activation of PPARG[16], and an increase in aldehyde dehydrogenase 1 family member A3 (ALDH1A3)[10] that contributes to their hyper-proliferative state. Loss of BMPR2 impairs PASMC motility[17], a feature important in the response to injury that is regulated by a transient BMPR2 dependent induction of CTNNB1 and activation of RHOA and RAC1[18]. Other studies have emphasized dysfunctional SMAD signaling[19], impaired contractile gene expression[20] and amplification of abnormalities with endothelin-1[21].

Transgenic mice with *Bmpr2* deletion in PAEC, develop hypoxia-induced pulmonary hypertension (PH) that persists after recovery in room air[13]. The impact of *Bmpr2* deletion in SMC (*BKO*^{smc}) on the development of pulmonary hypertension in mice had not been addressed primarily because there is considerable attrition of these mice owing to severe cardiac malformations[22]. However, the incomplete penetrance of the deletion in causing the cardiac defects allowed us to investigate the mechanism and severity of inducible PH in those mice whose phenotype appeared normal in the absence of intervention. To avoid the high attrition, we also created mice with an inducible *Bmpr2* knock-out in SMC (*iBKO*^{SMC}) that had a similar phenotype.

β-Arrestins are ubiquitous proteins initially described for their role in G protein-coupled receptor desensitization, sequestration, and internalization and serve as scaffold proteins for signaling molecules that regulate gene expression and cellular responses[23] including SMC proliferation in injured arteries[24]. β-arrestin 2 (ARRB2) is essential for the initiation and growth of intestinal tumors displaying elevated Wnt pathway activity[25], and β-arrestins act as signaling scaffolds for pAKT[26].

In this study we used chronic hypoxia not in association with lung disease but as a ‘second hit’ in mice with deletion of *Bmpr2* in SMC, much as could be encountered during exposure to high altitude, inflammation or sleep apnea[27]. We now show that PASMC with reduced BMPR2 exhibit heightened proliferation and impaired contractility, and persistent hypoxia-induced PH following return of these mice to room air. We relate these findings to increased pERK1/2-pP38-pSMAD2/3 upregulating ARRB2 and pAKT causing GSK3β inactivation and CTNNB1 mediated heightened proliferation, as well as reduced RHOA and RAC1 signaling that is responsible for impaired contractility. We show this relationship in human PASMC where we reduced BMPR2 by siRNA, and in PASMC of PAH patients with a

BMPR2 mutation. In the *iBKO*^{SMC} mouse model, inducible deleting one allele of *Arrb2* in SMC prevented persistent pulmonary hypertension after chronic hypoxia.

Methods

Data Availability

The authors declare that all supporting data are available within the article and its Supplemental Material. Additional methods or data related to this study are available from the corresponding authors upon reasonable request.

Expanded Methods are provided in the Data Supplement.

Transgenic Mice

Tagln-Cre/R26R/Bmpr2$^{-/-}$ mice (*BKO*^{SMC}), inducible *Acta2-CreER/Td/Bmpr2*$^{-/-}$ mice (*iBKO*^{SMC}) and *Acta2-CreER/Td/Bmpr2*$^{-/-}$*/Arrb2*$^{-/+}$ mice (*iBKO-iAHet*^{smc}) were created by breeding *Bmpr2*$^{flox/flox}$ with *Tagln-Cre, Acta2-CreER, R26R, Td-tomato*, or with *Arrb2*$^{flox/flox}$ mice. The mice were back-crossed for six generations onto a C57BL/6J background. Some *BKO*^{SMC} embryos at E19.5 were collected and fixed in 4% paraformaldehyde and heart defects evaluated by transverse and sagittal sections stained with H&E.

Mice at 8 weeks of age were housed under hypoxia (10% O_2) for three weeks, followed by four weeks of recovery in room air or were maintained in room air. The inducible knock-out mice and controls were fed a tamoxifen containing diet for four weeks[28] before exposure to hypoxia. The number of mice per experiment is indicated in the figure legends. Echocardiographic assessments of cardiac function, hemodynamic measurement of right ventricular (RV) systolic pressure (RVSP), histological and morphometric analyses of RV hypertrophy (RVH), and peripheral PA changes, were carried out as previously described[16]. Left ventricular end diastolic pressure (LVEDP)[29], LacZ[30] and Td-tomato staining were also performed as described in the Data Supplement.

Cell Culture

Primary murine (m) PASMC were isolated from mouse large PA following removal of the adventitia and EC layer[10] as described in the Expanded Methods in the Online Data Supplement. Human PASMC were isolated from small PA (<1mm) harvested from explanted lungs of PAH patients with a *BMPR2* mutation undergoing lung transplantation, and from unused donor lungs as controls[10], all obtained deidentified from the Pulmonary Hypertension Breakthrough Initiative (PHBI). Table S1 in the Data Supplement lists demographics, PAH hemodynamics and PAH medications. PASMC were cultured in Smooth Muscle Growth Medium (SMGM) as described[10]. For siRNA transfection or treatment by AngII or BMP4, PASMC were synchronized in starvation medium for 48 hours, then cultured in SMGM with 5% FBS.

Immunohistochemistry (IHC) and Morphometric Analysis

Paraffin-embedded mouse lung tissue sections (7 μm) were deparaffined and rehydrated following a standard protocol. Sections were blocked and permeabilized in the blocking buffer (3–5% BSA, 0.2% Triton X-100 in 1X TBS plus 5% Goat or Donkey serum) for one hour at room temperature, followed by standard protocol described in the Methods in the Data Supplement. Controls with only the secondary antibody were used to assess background and selectivity of staining. Images were acquired using a SPOT imaging system (SPOT IMAGING, Sterling Heights Headquarters, MI) connected to a Leica microscope (JH Technologies, Leica DMLB model, Fremont, CA).

Muscularization was assessed by comparing the number of muscularized PAs at alveolar duct and wall level (SPA) to the total number of arteries at these levels. The number of arteries at alveolar duct and wall level per 100 alveoli was also assessed. Analyses were done blinded to the experimental group to which the section belonged. For each mouse, we assessed six different sections representing different fields.

siRNA Transfection

Synchronized PASMC were transfected with nontargeting siRNA (siControl), or with siRNA targeting *BMPR2, ARRB2, CTNNB1*, or *SMAD2&3* using Lipofectamine RNAiMax for overnight. After siRNA transfection and synchronization, cells were cultured in SMGM for 48 hours, and treated as described for the various assays. siRNAs used in this study are listed in the Data Supplement.

PASMC Contraction Assay

Synchronized PASMC transfected with siRNA were cultured for 48 hours, then mixed with the collagen gel from Cell Biolabs, and loaded onto a 48-well plate (3×10^5 cells per 250 μL gel mix per well). After polymerization for 30 min at 37°C, the cells were cultured with SMGM and treatments added for 48–72 hours, the plates scanned and images obtained for gel contraction analysis. Residual gel area (mm^2) was measured using Fiji ImageJ. Wells containing gel without embedded PASMC were included as un-contracted controls.

Proliferation and Survival Assays

Proliferation assessed by cell count: Equal numbers of PASMC were seeded in 24-well plates, cultured with 5% FBS in SMGM, and counted using a cell counter.

Proliferation by the MTT assay (ATCC): Cells were cultured in 96-well plates following incubation with MTT solution at 37°C for 3 hours, and OD read by Microplate Reader.

Survival: Survival following serum withdrawal was assessed by cell counts in 24-well plates and by luminescence using the Caspase-Glo® 3/7 Assay kit (Promega) in 96-well plates.

Real Time PCR

Total RNA was isolated using the Zymo Research Quick-RNA MiniPrep Kit. The quantity and quality of RNA was determined by using a spectrophotometer, and RNA was reverse transcribed using the High Capacity RNA to cDNA Kit (Applied Biosystems). Expression level of genes was normalized to the expression level of *Actb* mRNA (for mouse) or *ACTB* mRNA (for human). Detailed methods and primers' information are available in the Data Supplement and in the Major Resources Table.

Protein Analysis by Western Immunoblot

Protein concentration was determined using the Pierce BCA assay. Catalog numbers and dilutions of the antibodies are detailed in the Data Supplement and in the Major Resources Table. Proteins were run on an SDS polyacrylamide gel and transferred to a nitrocellulose membrane. Western immunoblot was performed as described in the Data Supplement. Protein Levels were assessed relative to loading-control (GAPDH or tubulin).

Active RHOA and RAC1 Pull Down Assays

Assays were carried out on 500 μg protein from freshly prepared lysates using the Thermo Scientific Pierce active RHO and active RAC1 Pull-Down and Detection Kits. Western immunoblot detection was performed as described in the Data Supplement[31].

Immunofluorescence on Tissue and PASMC

Human or mouse lung tissue sections (7 μm) embedded in paraffin were deparaffinized and rehydrated following standard protocols. Following the Antigen retrieval, sections were blocked and permeabilized for one hours, and were incubated with primary antibody for overnight followed by fluorescent conjugated IgG secondary antibody. Controls with the secondary antibody only were used to assess background and selectivity of staining. The catalog numbers and dilutions of the antibodies are provided in the Data Supplement and the Major Resources Table. Nuclei were stained with DAPI. Images were acquired using a Leica TCS SP8 confocal microscope. Positive staining on lung sections was based on colocalization with a smooth muscle cell marker and the location of the protein of interest was noted as cytoplasmic or nuclear.

Filament actin Immuno-staining was carried out on fixed PASMCs described in the Data Supplement. Filament actin was stained with DyLight 488 Phalloidin and nuclei were stained with DAPI. Images were acquired on an Olympus Fluoview FV1000 confocal microscope. For assessment of actin filaments, average F-actin per cell was quantified as total F-actin pixels divided by the number of nuclei in each field, using Fuji ImageJ.

Analyses were done blinded to the experimental group to which the section belonged.

The confocal immunofluorescent images were taken from immunostaining done at the same time and under the same conditions for a given experiment. Images that best represented the average level of each marker for each condition studied were selected for display in the figures.

Ratio of F-ACTA2 to G-ACTA2 Assay

siRNA transfected PASMC were treated with AngII (4 μM) or PBS for 6 hours. Cells were harvested with LAS2 buffer from the G/F-ACTA2 Cytoskeleton In Vivo Assay kit. The F/G ACTA2 ratio assay was performed as previously described[31], and F-ACTA2 and G-ACTA2 assessed by western immunoblot.

Statistical Analysis

Data was analyzed using GraphPad Prism version 9.0 for Mac OS X, GraphPad Software, San Diego, CA, USA, www.graphpad.com. For samples with an $n \geq 6$, the Shapiro-Wilk normality test was first applied. As all data with an $n \geq 6$ passed this normality test, they were analyzed by either parametric t-test with Welch's correction (unpaired and two-tailed) for two groups; by parametric 1-way ANOVA for more than two groups; or by 2-way ANOVA for comparisons of multiple conditions applied to two or more groups, with adjustment for multiple comparisons using Tukey's post hoc test. As a small sample size with an $n<6$ cannot be reliably tested for normality, we used a non-parametric test, either the Kolmogorov-Smirnov t-test (unpaired and two-tailed) when two groups were being compared, or the one-way ANOVA Kruskal-Wallis test for more than two groups, adjusted for multiple comparisons using the Dunn's post hoc test. A *P*-value of <0.05 was considered significant. For comparisons with n=3 we indicate where the minimum achievable *P*-value of 0.1000 was reached using the non-parametric test.

No experiment-wide/across-test multiple test correction was applied in this study. The normality test, subsequent hypothesis tests, the exact p values and sample size are presented in Table S2.

Study Approvals

The Animal Care Committee of Stanford University approved all protocols, in keeping with the regulations of the American Physiological Society. Procurement of the tissues from human subjects is approved by the Administrative Panel on Human Subjects in Medical Research at Stanford University (IRB # 350, Panel 6).

Results

Tagln-Cre/Bmpr2$^{-/-}$ Mice Show Decreased Acute Hypoxic Vasoconstriction, and Persistent Pulmonary Hypertension after Chronic Hypoxia

To determine whether loss of BMPR2 in PASMC contributes to PH, we created SMC specific *Bmpr2*$^{-/-}$ (*BKO*^{SMC}) by crossing *Bmpr2* floxed with *Tagln*-Cre mice carrying a ROSA Cre activity reporter. Genotyping and LacZ staining confirmed knockout of *Bmpr2* in vascular SMC (Figure 1A and Figure S1A). About half of the *BKO*^{SMC} mice died shortly after birth. Image analysis of serial sectioning of the heart and lung tissues in the *BKO*^{SMC} embryos at 19.5 days (E19.5) revealed, as previously reported[22], mice with lethal heart defects (Figure S1B).

We investigated the response to hypoxia of *BKO*^{SMC} survivors and wild-type (WT) littermates. Eight-week-old mice were exposed to three weeks of hypoxia (10% O_2)

followed by four weeks of recovery in normoxia, and compared to mice maintained in normoxia. *BKO*^{smc} male mice had reduced acute hypoxia-induced pulmonary vascular reactivity (Figure 1B) and while they developed features of less severe PH following chronic hypoxia, they had persistent PH following recovery in normoxia when compared to WT littermates, as assessed by right ventricular systolic pressure (RVSP) (Figure 1C). These findings were consistent with right ventricular hypertrophy (RVH) assessed by an increase in the weight of the right ventricle/left ventricle + septum (RV/LV+S) (Figure 1D) and a reduced pulmonary artery acceleration time (PAAT) assessed by 2D-echocardiograpy (Figure S1C), and were in keeping with persistent muscularization of distal pulmonary arteries (PA) (Figure 1E). There was no statistically significant difference in the number of distal PAs per 100 alveoli compared with WT mice, suggesting no loss of distal PA (Figure S1D). The *BKO*^{SMC} male mice had slightly reduced left ventricular fractional shortening (LVFS), ejection fraction (LVEF) and cardiac output (LVCO) under hypoxia but echocardiographic findings were similar to WT mice after recovery (Figure S1E–S1H). These results indicate that loss of BMPR2 in murine PASMC contributes to the persistence of hypoxia induced PH, related to increased PA muscularity, despite decreased vasoreactivity.

The *BKO*^{SMC} female mice had a somewhat less severe hemodynamic response to chronic hypoxia as previously described in rats[32] and no differences were detected in the *BKO*^{SMC} vs. WT controls potentially because of the small size of the female cohort (Figure S2A, S2B, S2C).

BKO^{SMC} PASMC Display Increased Proliferation and Survival, and Reduced Contractility

To understand how loss of BMPR2 reduced hypoxic vasoreactivity but induced more persistent muscularity in the *KO*^{SMC} mouse, we harvested SMC from the large PA of male *BKO*^{SMC} and WT littermates. We confirmed the reduction of *Bmpr2* in cultured murine PASMC by LacZ staining and quantitative real time PCR (Figure 2A). Approximately 10–15% of cultured cells were negative for LacZ staining likely due to some variability in Cre activity, leading to incomplete deletion of the floxed target gene. PASMC from *BKO*^{SMC} compared to those from WT mice showed an increase in proliferation assessed by MTT (Figure 2B) and resistance to apoptosis by caspase assay (Figure 2C), and by cell counts for both proliferation and survival (Figure S3A, S3B). We selected angiotensin (Ang) II[33] and BMP4[34] as stimuli to test PASMC contractility. There was reduced contractility in response to vehicle, AngII (4 μM) and BMP4 (10 ng/mL) as assessed by the gel contraction assay as greater residual gel area (Figure 2D) in PASMC from *BKO*^{SMC} vs. WT mice.

Active β-catenin (ABC) promotes proliferation and survival of cultured SMC, and its expression and activity are induced during vascular remodeling[10,35]. We found elevated total β-catenin (CTNNB1) and ABC in PASMC of *BKO*^{SMC} vs. WT mice (Figure 2E) that we related to increased proliferation of PASMC, since this feature was reduced following treatment with siRNA targeting *Cnntb1* (Figure 2F top).

Previous studies from our laboratory demonstrated that BMP2 stimulates PASMC migration via BMPR2-dependent activation of RHOA and RAC1[18]. RHOA signaling affects contractility of pulmonary SMC from rats with chronic PAH[36] and plays a general role in

maintenance of SMC differentiation[37]. Others showed that expression of dominant negative RHOA abrogated apical actin assembly[38]. We found reduced active RHOA and active RAC1 in *BKO*^{SMC} PASMC at baseline and in response to AngII (Figure 2G, 2H) that was consistent with their decreased contractility. To better understand the role of BMPR2 in the regulation of SMC contractility, we examined representative SMC contractile proteins, smooth muscle alpha actin (ACTA2), smooth muscle *protein* alpha of 22 kDa (TAGLN), and calponin (CNN1). Expression of TAGLN and ACTA2 was reduced in the *BKO*^{SMC} PASMC, while the expression of CNN1 was not significantly changed (Figure S3C).

Loss of BMPR2 in Human PASMC Leads to ARRB2 Dependent Activation of pAKT and ABC Causing Enhanced Proliferation and Survival

We next determined whether human PASMC would also show a pro-proliferative, hypocontractile PASMC phenotype in response to loss of BMPR2 and further addressed the mechanism involved. When BMPR2 was reduced by siRNA (si*BMPR2*) in small human PASMC, a hyper-proliferative phenotype was evident as judged by the MTT assay (Figure 3A) and by cell counts (Figure S4A) and this was accompanied by enhanced survival in response to serum withdrawal, assessed by the caspase activity assay (Figure 3B) and by cell counts (Figure S4B). Interestingly DNA damage was slightly reduced in normoxia but increased with hypoxia and with reoxygenation in the PASMC with *BMPR2* siRNA (Figure S4C). Improved cell survival in normoxia was not associated with increased DNA damage.

We previously showed that the ligand BMP2 only transiently increased ABC in human PASMC via pAKT-mediated phosphorylation and inactivation of GSK-3β[18] but that ABC was required for the increase in NFY, a transcription factor that regulates cell cycle genes in PAH PASMC[10]. Reducing BMPR2 by siRNA increased phosphorylation of GSK-3β at Serine 9, increasing the level of inactive GSK-3β [pGSK-3β(S9)] and ABC, without a change in other molecules complexed with ABC such as disheveled (DSH) or Axin (AXIN) (Figure 3C).

ARRB2 interacts with AXIN and DSH after Wnt3A stimulation of mouse embryo fibroblasts, resulting in GSK-3β inactivation and ABC stabilization[39]. Based on these findings, we hypothesized that loss of BMPR2 in PASMC results in an increase in ARRB2, pAKT and pGSK-3β(S9) mediated activation of CTNNB1. Indeed, ARRB2 was increased in PASMC with reduced BMPR2 by siRNA whereas ARRB1 was unchanged (Figure 3D). This was accompanied by an increase in pAKT(Ser473), pGSK-3β(S9) and ABC at baseline or following AngII stimulation. Further studies probing the isoform involved indicated that there was an increase in pAKT1 recognized by the Ser473 antibody (Figure S4D). Moreover, decreasing *ARRB2* by siRNA attenuated the heightened pAKT(Ser473), pGSK-3β(S9) and ABC (Figure 3E), suggesting that ARRB2 is upstream of pAKT(Ser473), pGSK-3β(S9) and ABC in stimulating the hyperproliferative phenotype that results from loss of BMPR2.

We confirmed that pAKT(Ser473) is downstream of ARRB2 and upstream of pGSK-3β(S9), by inhibition of pAKT kinase activity using GSK690693, currently in clinical development for patients with various malignancies[40]. PASMC were treated with si*BMPR2* or siControl for 48 hours, then with GSK690693 (2 μM and 10 μM) for 48 hours. Down-regulation

of pGSK-3β(S9) was attributed to inhibition of pAKT activity, despite accumulation of pAKT(Ser473) protein (Figure S4E).

We next tested if the ARRB2-pAKT-ABC pathway regulated proliferation. Indeed, reducing ARRB2 or CTNNB1 attenuated the increased proliferation in human PASMC with reduced BMPR2 (Figure S4F, S4G). Taken together, our results indicate that loss of BMPR2 in human PASMC causes ARRB2-dependent activation of pAKT and ABC, related to their pro-proliferative and anti-apoptotic phenotype.

Loss of BMPR2 increases ARRB2 via pERK-pP38-SMAD2/3

We next determined whether the loss of BMPR2 mediates an increase in ARRB2 via enhanced pERK, pP38 and/or SMAD2/3[19] expression. Reducing SMAD2 or SMAD3 by siRNA in in *BMPR2* deficient cells (Figure S4H) decreased ARRB2 and downstream effector ABC at the protein level without affecting pP38 (Figure 4A). However, when pP38 catalytic activity (not protein) was reduced by SB203580[41] pSMAD2/3 was reduced but not pERK (Figure 4B). Further, when pERK was inhibited by PD98059, pP38, pSMAD2/3 and ARRB2 and ABC were decreased (Figure 4C). This suggests an axis whereby pERK activates pP38 to increase pSMAD2/3 resulting in elevated levels of ARRB2 and, as a consequence, ABC (Figure 4C, schema).

Loss of BMPR2 Reduces Human PASMC Contractility via ARRB2 Dependent RHOA/RAC1 and Reduction in Actin Stress Fibers

BMP signaling promotes SMC contractile proteins[34] and facilitates PASMC motility[17]. RHOA regulates the formation of actin stress fibers and focal adhesions[42]. Inactivation of RHOA is essential for the reduction of tension and contractility[31]. We assessed contractility, RHOA and RAC1 at baseline and in response to AngII stimulation in PASMC with reduced BMPR2 by siRNA. We observed reduced contraction, measured by a gel contraction assay (Figure 5A), and decreased total and active RHOA and RAC1 by immunoblot (Figure 5B, 5C), similar to the phenotype observed in murine PASMC from the BKO^{SMC} mice.

We examined representative contractile proteins in PASMC treated with si*BMPR2.* Expression of TAGLN was reduced in PASMC with loss of *BMPR2*, while the expression of ACTA2, CNN1 were not significantly altered (Figure S5A). TAGLN binds filament (F)-ACTA2 stress fibers and is important in their organization[43]. As judged by Phalloidin immunofluorescent staining, F-ACTA2 stress fibers were decreased in human PASMC with reduced BMPR2, and the enhanced production of F-ACTA2 in response to Angiotensin II stimulation was attenuated (Figure 5D). This is consistent with a reduced filament- to globule-ACTA2 ratio (F/G ACTA2) in PASMC with loss of BMPR2. (Figure S5B).

To further relate the reduced contractile phenotype to the increase in ARRB2, we investigated PASMC transfected with si*BMPR2,* si*ARRB2* or both, at baseline and in response to AngII stimulation. Reducing *ARRB2* by siRNA prevented the decrease in RHOA and RAC1 (Figure 6A) and improved the contractility of PASMC with reduced *BMPR2* (Figure 6B). The decrease in TAGLN was reversed, without significant impact on ACTA2 and CNN1 (Figure S5A). Taken together, our data suggest that the impaired contractility caused by loss of BMPR2 in human PASMC is related to an ARRB2-dependent

reduction of RHOA, RAC1 and TAGLN, that leads to the destabilization of actin stress fibers.

PASMC in PAH-*BMPR2$_{Mut}$* Displayed Abundant ARRB2 and ABC Protein Associated with Enhanced Proliferation and Survival

We then extended our investigation to PASMC from PAH patients with a *BMPR2* mutation (PAH-*BMPR2$_{Mut}$*), harvested from lungs removed at transplant from PAH-*BMPR2$_{Mut}$* patients, and from unused donor lungs as controls. Demographic and hemodynamic information are provided in Table S1. Confocal microscopic analysis revealed that the expression of both ARRB2 (in the cytoplasm) and ABC (in nuclei) were abundant in the small PASMCs in PAH-*BMPR2$_{Mut}$* compared with donor control lungs (Figure 7A, 7B). In agreement with our findings in PASMC where BMPR2 was reduced by siRNA, PASMC from PAH-*BMPR2$_{Mut}$* patients displayed elevated proliferation and apoptosis resistance compared to donor controls (Figure S6A–S6D). This was associated with an increase in ARRB2, pAKT and ABC in the PAH-*BMPR2$_{Mut}$* PASMC (Figure 7C). Reducing ARRB2 by siRNA in PAH-*BMPR2$_{Mut}$* PASMC significantly decreased pAKT and ABC (Figure 7D). Inhibiting pAKT phosphorylation activity with GSK960963[40] (2 μM and 10 μM) caused accumulation of pAKT and ARRB2 (at higher dose), and reduced pGSK-3β(S9) (Figure S6E). The enhanced proliferation of PAH-*BMPR2$_{Mut}$* PASMC vs. donor control PASMC was suppressed by reducing ARRB2 and CTNNB1 with siRNA (Figure 7E, 7F), and by inhibition of pAKT activity with GSK690693 (Figure S6F).

PASMC from PAH-*BMPR2$_{Mut}$* Show Reduced Contractility, Related to Increased ARRB2 and Reduced RHOA/RAC1

Similar to our findings with loss of BMPR2 in PASMC, we found decreased contractility in PAH-*BMPR2$_{Mut}$* PASMC compared with donor PASMC (Figure 8A), with lower RHOA and RAC1, and an attenuated response to AngII stimulation (Figure 8B, 8C). Furthermore, reducing ARRB2 by si*ARRB2* increased RHOA and RAC1 in the PAH-*BMPR2$_{Mut}$* PASMC (Figure 8D).

In summary our studies in human PASMC with mutant or reduced BMPR2, show that the consequent increase in ARRB2 results in pAKT-GSK3β(S9)-mediated activation of CTNNB1, that is responsible for the hyperproliferative phenotype and that ARRB2 dependent reduction in RHOA/RAC1, TAGLN and in actin stress fibers causes hypocontractility (Schema in Figure 8E).

Reducing *Arrb2* in SMC Prevents the Development of PH in *iBKO-iAHet^{smc}* Mice

Because of the prenatal attrition of the *BKO^{SMC}* mice, we created a tamoxifen inducible model for the next series of studies, *Acta2-CreER/Td/Bmpr2$^{-/-}$* (*iBKO^{SMC}*). These mice allowed us to investigate whether reducing *Arrb2* prevents the development of PH in the *iBKO^{SMC}* mice, by also generating inducible *Acta2-CreER/Td/Bmpr2$^{-/-}$/Arrb2$^{-/+}$* mice (*iBKO-iAHet^{SMC}*).

We assessed the response of *iBKO^{SMC}* mice, *iBKO-iAHet^{SMC}* mice, and control mice (iWT) to hypoxia and recovery in room air vs room air. Mice 6–7 weeks of age were fed

Tamoxifen in their diet for 4 weeks, followed by exposure to hypoxia (10% O_2) for three weeks and four weeks of recovery in room air, and compared to mice at similar age and genotype maintained in room air (Figure 9A). Deletion of *Bmpr2* and one allele of *Arrb2* in PASMC was evident by PCR genotyping and co-localization of ACTA2 and Td-tomato. The detailed confocal images demonstrated Td-tomato expression in SMC but not in the EC in tissue sections (Figure S7A and Figure 9B). We confirmed by RT-qPCR that the major reduction in BMPR2 occurs in SMC with no statistically significant difference in PAEC and minor reductions in the heart and lungs consistent with the presence of SMC in these tissues (Figure S7B). The *iBKO*^{SMC} mice exhibited a phenotype similar to the *BKO*^{SMC} mice, assessed by impaired vasoreactivity judged in relation to norepinephrine, and reduced chronic hypoxia induced PH, but impaired resolution of PH with reoxygenation judged by elevated RVSP (Figure 9C, 9D), echocardiographic determination of reduced PAAT (Figure S7C), and RVH (Figure 9E), associated with heightened muscularity in distal PAs (Figure 9F). There was no significant difference in the number of distal PAs per 100 alveoli compared with iWT under same condition (Figure S7D). The *iBKO-iAHet*^{SMC} mice, however, displayed a phenotype similar to the iWT mice (Figure 9D–F and Figure S7C and D), suggesting that deletion of one allele of *Arrb2* in *iBKO*^{SMC} prevented persistent PH during recovery. Further immunoblot analysis of the PAs revealed that *iBKO-iAHet*^{SMC} mice had a normal ARRB2 expression level, resulting in restoration of ABC and RHOA expression in the PAs to the iWT levels (Figure 9G). Moreover, immunofluorescent analysis of lung tissue sections of the recovery cohort showed an increase in pAKT(Ser473) and Ki67 in the *iBKO*^{SMC} vs. *iBKO-iAHet*^{SMC} *and control mice* (Figure 9H and Figure S7E respectively). In these studies, the *iBKO*^{SMC} female mice were similar to the males in the reduced hypoxia induced and persistent PH during recovery in Room Air (Figure S7F, G, H), and LV function including LVEDP were similar in all cohorts in males and females (Figure S8A–S8I). *iAHet*^{SMC} were similar to controls under normoxia, following chronic hypoxia, and reoxygenation in room air (Figure S9). While a contribution of fibroblasts with deletion of BMPR2 could not be completely ruled out, our previous study deleting BMPR2 specifically in fibroblasts using a *Col1A2-CreER* inducible *Bmpr2* KO mouse showed not significant differences in the PH phenotype comparing with iWT mice (Figure S9).

Discussion

In this study we found that PASMC with loss of BMPR2 are hypocontractile, hyper-proliferative and resistant to apoptosis, features that can explain lack of resolution of structural remodeling and persistent pulmonary hypertension after an inducing stimulus like hypoxia even unrelated to lung disease. These findings suggested that deficiency of BMPR2 in PASMC can contribute to the development of PAH. The role of loss of BMPR2 in other cells, such as bone marrow derived cells, is also important to investigate since bone marrow transplantation of *Cav1* mutant mice was sufficient to prevent pulmonary hypertension[44].

As TAGLN is expressed in cardiomyocytes early in development[45], it is not surprising that *Bmpr2* deletion by *Tagln*-Cre causes heart defects[46]. It is unknown why there is incomplete penetrance of the lethal phenotype and only mildly impaired cardiac function under chronic hypoxia. The impaired contractility of PASMC appears to account for the reduced PA vasoconstriction observed in response to acute hypoxia, likely accounting for

the slight decrease in right ventricular systolic pressure during chronic hypoxia. Similar muscularization of distal arteries under hypoxia despite lower pressures in the *BKO*^{SMC} mice could be attributed to the enhanced proliferation of PASMC, whereas the sustained PH in the mice with loss of BMPR2 in PASMC is consistent with the reduced propensity to apoptosis of PASMC that is associated with regression of chronic hypoxia-induced PH. Interestingly, sustained hypoxia-induced PH after return to room air is also evident in transgenic mice with *Bmpr2*[13] or *Pparg*[47] deleted in EC, and appears to reflect the contribution of EC to hyperproliferative phenotype of SMC. In the clinical setting reduced BMPR2 can worsen even transient hypoxic PH[27].

We attribute the relationship of heightened proliferation and resistance to apoptosis to CTNNB1 mediated gene regulation. We previously showed transient expression of CTNNB1 in response to BMP2 stimulation and pAKT(Ser473) inactivation of GSK3β[18]. Based upon these studies, we pursued the role of pAKT(Ser473) in the activation of CTNNB1. Sustained expression of CTNNB1 was posited to lead to enhanced PASMC proliferation in response to growth factors such as PDGF[16]. In these studies, it was shown that mutant DVL that could not interact with RHOA and RAC1 allowed for persistent activation of CTNNB1, explaining both impairing contractility and the propensity for heightened proliferation particularly in response to growth factors such as PDGF[16,18]. Targeting this pathway has been effective in preventing experimentally induced neointimal formation in systemic arteries[48].

We recently reported that the hyperproliferative phenotype of PAH PASMC is related to CTNNB1-TCF-LEF mediated upregulation of ALDH1A3 and nuclear transcription factor Y subunit alpha (NFYA)[10], and those genes regulated by NFYA that include metabolic enzymes necessary for glycolytic metabolism and cell cycle genes important in cell division[10].

In addition to classical functions downstream of G-protein coupled receptors, β-arrestins function as scaffolding signaling molecules in a number of growth factor mediated pathways[26]. In endothelial cells, VEGFR3 requires ARRB1 for angiogenic function, related in part to phosphorylation of endothelial nitric oxide synthase[49] and *Arrb1*$^{-/-}$ mice had worse hypoxia induced PH[49]. ARRB2 has been linked to BCL2 associated agonist of cell death (BAD) phosphorylation and resistance to apoptosis in rat SMC[50]. Another study showed that loss of *Arrb2* in low-density lipoprotein receptor-deficient mice (*Ldlr*$^{-/-}$) fed a high fat diet are protected from atherogenesis and *Arrb2*$^{-/-}$ mice are protected from thickening of the vessel wall due to injury, compared with wild type mice[24]. In addition, there is an interaction between ARRB2 and DVL that could support a displaced interaction with RHO and RAC[51] leading to their destabilization. Arrestins have also been directly implicated in RHO and RAC mediated focal adhesion formation in HEK293T cells and mouse embryonic fibroblasts[52].

Vascular SMC, unlike other muscle cells, do not terminally differentiate, and in response to injury, generally de-differentiate resulting in loss of contractility and abnormal proliferation, migration, and extracellular matrix production[34,53]. On the other hand, normal laminar shear stress induces synthetic to contractile phenotypic modulation of vascular SMC[54]. Dysregulation of SMC growth and differentiation could lead to pathological remodeling

of the vessel wall. Indeed, BMP signaling inhibits vascular SMC proliferation[55], and microarray analysis of lung tissue from mice expressing dominant negative *Bmpr2* in SMC revealed decreased SMC differentiation markers[20]. In conclusion, our study reveals an independent contribution of BMPR2 in SMC to the pathology associated with PAH and a BMPR2 mutation. Strategies to augment BMPR2 signaling should consider the contribution of SMC as well as EC BMPR2 in reversing the pathology of PAH.

Supplementary Material

Refer to Web version on PubMed Central for supplementary material.

Acknowledgments

We greatly appreciate the editorial assistance of M.B. Roof in preparing the figures and text, and the administrative help of M. Ameri. The Graphical Abstract and schemas in the figures were partly generated using Servier Medical Art, provided by Servier, licensed under a Creative Commons Attribution 3.0 unported license. We thank Dr. Hirofumi Sawada for helping with Echocardiographic assessments for part of the *Tagln-Cre/BMPR2*$^{-/-}$ mice; Ms. Audey Shen for immunofluorescent staining and confocal image analysis of F-Actin in human PA SMC; Dr. Tushar Desai for providing access to the confocal microscope; Dr. Dan Bernstein for the use of the cardiac phenotyping equipment; Grégory Scherrer (University of North Carolina at Chapel Hill, G.S. is a NYSCF – Robertson Investigator) for providing the *Arrb2*-floxed mice and the genotyping methodology; and Dr. Maya Kumar for transferring the *Acta2-CreER* mice. We are indebted to the Pulmonary Hypertension Breakthrough Initiative (PHBI), funded by NIH/NHLBI R24 HL123767 and the Cardiovascular Medical Research and Education Fund (CMREF) UL1 RR024986, as the source of cells and tissues from PAH patients and unused donor controls. Deidentified demographic and clinical data were supplied by the Data Coordinating Center at the University of Michigan and we thank Ms. Patricia A. del Rosario for obtaining these data.

Sources of Funding

This work was supported by the NIH/NHLBI R01 HL074186 (Marlene Rabinovitch). The PHBI was funded by NIH/NHLBI grant R24 HL123767 and the Cardiovascular Medical Research and Education Fund (CMREF) grant UL1RR024986. J.R. Moonen was supported by the California TRDRP of the University of California award 27FT-0039, and by the Netherlands Heart Foundation award 2013T116. S. Taylor was supported by NIH/NHLBI T32 Fellowship in Pulmonary Medicine T32 HL129970 and NIH/NHLBI Research Diversity Supplement P01 HL108797–04W1. S. Isobe was supported by Fellowshops from the MSD Life Science Foundation Fellowship, the American Heart Association (award number 20POST35080009), and the Japan Society for the Promotion of Science. D. Marciano is supported by NIH-NHLBI grant K99 HL 1450970. D. Li was supported by an American Lung Association Senior Research Training Fellowship RT-509274. M. Gu is supported by NIH/NHLBI grant K99/R00 HL135258. M. Rabinovitch is also supported by the Dwight and Vera Dunlevie Chair in Pediatric Cardiology at Stanford University.

Non-standard Abbreviations and Acronyms

ABC	Active beta-catenin
***BKO*^{SMC}**	*Bmpr2* knock-out in smooth muscle cell (*Tagln-Cre/Bmpr2*$^{-/-}$)
EC	Endothelial cell
F-ACTA2	Filamentous alpha actin
G-ACTA2	Globular / monomeric alpha actin
GST-RBD	GST fusion protein of the Rhotekin binding domain
GST-PBD	GST fusion protein of the Pak1 binding domain

IF	Immunofluorescence
IPAH	Idiopathic pulmonary arterial hypertension
iBKO^{SMC}	Mice with tamoxifen-inducible *Bmpr2* knock-out in smooth muscle cells (*Acta2-CreER/Td tomato/Bmpr2$^{-/-}$*)
iBKO-iAHet^{SMC}	Mice with tamoxifen-inducible knock-out of both *Bmpr2 alleles* and one *Arrb2* allele in smooth muscle cells (*Acta2-CreER/Td/Bmpr2$^{-/-}$/Arrb2$^{-/+}$*)
iBKO^{Fibro}	Mice with tamoxifen-inducible *Bmpr2* knock-out in fibroblast cells (*Col1A2-CreER/R26R/Bmpr2$^{-/-}$*)
PAAT	Pulmonary arterial acceleration time
PA	Pulmonary artery
PAEC	Pulmonary artery endothelial cells
PAH	Pulmonary arterial hypertension
PASMC	Pulmonary artery smooth muscle cells
PH	Pulmonary hypertension (refers to mouse experiments)
pGSK3-β	Phospho- glycogen synthase kinase 3- beta (inactive)
pERK	Phosphorylated extracellular signal related kinase
pAKT	Phosphorylated protein kinase B
PCR	Polymerase chain reaction
RT-qPCR	Real time quantitative polymerase chain reaction
RVSP	Right ventricular systolic pressure
RVH	Right ventricular hypertrophy
RV/LV+S	Right ventricle/left ventricle + septum (weight ratio)
R26R	Rosa 26 Reporter transgene
siRNA	Small interference RNA
SMC	Smooth muscle cell
SMGM	Smooth Muscle Growth Medium
Td	Td tomato reporter transgene
WT	Wild-type control mice included *Tagln-Cre^{+}/R26R^{+}* and *Tagln-Cre^{-}/R26R^{+}/Bmpr2$^{f/f}$* littermates.

iWT	Control mice for Tamoxifen-inducible models. The following genotypes were used: *Acta2-CreER^{+}/Td^{+}* and *Td^{+}/Bmpr2$^{f/f}$* littermates for the *iBKO^{SMC}*, *Acta2-CreER^{+}/Td^{+}* and *Td^{+}/Bmpr2$^{f/f}$/Arrb2$^{f/+}$* littermates for *iBKO-iAHet^{SMC}*, or *Col1A2-CreER^{+}/Td^{+}* and *Td^{+}/Bmpr2$^{f/f}$* littermates for the *iBKO^{Fibro}* mice.

References:

1. Rabinovitch M Molecular pathogenesis of pulmonary arterial hypertension. J Clin Invest. 2012;122:4306–4313. doi: 60658 [pii] 10.1172/JCI60658 [PubMed: 23202738]
2. Lane KB, Machado RD, Pauciulo MW, Thomson JR, Phillips JA 3rd, Loyd JE, Nichols WC, Trembath RC. Heterozygous germline mutations in BMPR2, encoding a TGF-beta receptor, cause familial primary pulmonary hypertension. Nat Genet. 2000;26:81–84. doi: 10.1038/79226 [PubMed: 10973254]
3. Deng Z, Haghighi F, Helleby L, Vanterpool K, Horn EM, Barst RJ, Hodge SE, Morse JH, Knowles JA. Fine mapping of PPH1, a gene for familial primary pulmonary hypertension, to a 3-cM region on chromosome 2q33. Am J Respir Crit Care Med. 2000;161:1055–1059. [PubMed: 10712363]
4. Soubrier F, Chung WK, Machado R, Grunig E, Aldred M, Geraci M, Loyd JE, Elliott CG, Trembath RC, Newman JH, et al. Genetics and genomics of pulmonary arterial hypertension. J Am Coll Cardiol. 2013;62:D13–21. doi: 10.1016/j.jacc.2013.10.035 [PubMed: 24355637]
5. Atkinson C, Stewart S, Upton PD, Machado R, Thomson JR, Trembath RC, Morrell NW. Primary pulmonary hypertension is associated with reduced pulmonary vascular expression of type II bone morphogenetic protein receptor. Circulation. 2002;105:1672–1678. [PubMed: 11940546]
6. Alastalo TP, Li M, Perez Vde J, Pham D, Sawada H, Wang JK, Koskenvuo M, Wang L, Freeman BA, Chang HY, et al. Disruption of PPARgamma/beta-catenin-mediated regulation of apelin impairs BMP-induced mouse and human pulmonary arterial EC survival. J Clin Invest. 2011;121:3735–3746. doi: 10.1172/JCI43382 [PubMed: 21821917]
7. Kim J, Kang Y, Kojima Y, Lighthouse JK, Hu X, Aldred MA, McLean DL, Park H, Comhair SA, Greif DM, et al. An endothelial apelin-FGF link mediated by miR-424 and miR-503 is disrupted in pulmonary arterial hypertension. Nat Med. 2013;19:74–82. doi: 10.1038/nm.3040 [PubMed: 23263626]
8. Hopper RK, Moonen JR, Diebold I, Cao A, Rhodes CJ, Tojais NF, Hennigs JK, Gu M, Wang L, Rabinovitch M. In Pulmonary Arterial Hypertension, Reduced BMPR2 Promotes Endothelial-to-Mesenchymal Transition via HMGA1 and Its Target Slug. Circulation. 2016;133:1783–1794. doi: 10.1161/CIRCULATIONAHA.115.020617 [PubMed: 27045138]
9. Miyagawa K, Shi M, Chen PI, Hennigs JK, Zhao Z, Wang M, Li CG, Saito T, Taylor S, Sa S, et al. Smooth Muscle Contact Drives Endothelial Regeneration by BMPR2-Notch1-Mediated Metabolic and Epigenetic Changes. Circ Res. 2019;124:211–224. doi: 10.1161/CIRCRESAHA.118.313374 [PubMed: 30582451]
10. Li D, Shao NY, Moonen JR, Zhao Z, Shi M, Otsuki S, Wang L, Nguyen T, Yan E, Marciano DP, et al. ALDH1A3 Coordinates Metabolism with Gene Regulation in Pulmonary Arterial Hypertension. Circulation. 2021. doi: 10.1161/CIRCULATIONAHA.120.048845
11. Li CG, Mahon C, Sweeney NM, Verschueren E, Kantamani V, Li D, Hennigs JK, Marciano DP, Diebold I, Abu-Halawa O, et al. PPARgamma Interaction with UBR5/ATMIN Promotes DNA Repair to Maintain Endothelial Homeostasis. Cell Rep. 2019;26:1333–1343 e1337. doi: 10.1016/j.celrep.2019.01.013 [PubMed: 30699358]
12. Hennigs JK, Cao A, Li CG, Shi M, Mienert J, Miyagawa K, Korbelin J, Marciano DP, Chen PI, Roughley M, et al. PPARgamma-p53-Mediated Vasculoregenerative Program to Reverse Pulmonary Hypertension. Circ Res. 2021;128:401–418. doi: 10.1161/CIRCRESAHA.119.316339 [PubMed: 33322916]
13. Diebold I, Hennigs JK, Miyagawa K, Li CG, Nickel NP, Kaschwich M, Cao A, Wang L, Reddy S, Chen PI, et al. BMPR2 preserves mitochondrial function and DNA during reoxygenation to

promote endothelial cell survival and reverse pulmonary hypertension. Cell Metab. 2015;21:596–608. doi: 10.1016/j.cmet.2015.03.010 [PubMed: 25863249]

14. Meloche J, Pflieger A, Vaillancourt M, Paulin R, Potus F, Zervopoulos S, Graydon C, Courboulin A, Breuils-Bonnet S, Tremblay E, et al. Role for DNA damage signaling in pulmonary arterial hypertension. Circulation. 2014;129:786–797. doi: 10.1161/CIRCULATIONAHA.113.006167 [PubMed: 24270264]
15. Sutendra G, Bonnet S, Rochefort G, Haromy A, Folmes KD, Lopaschuk GD, Dyck JR, Michelakis ED. Fatty acid oxidation and malonyl-CoA decarboxylase in the vascular remodeling of pulmonary hypertension. Sci Transl Med.2:44ra58. doi: 2/44/44ra58 [pii] 10.1126/scitranslmed.3001327
16. Hansmann G, de Jesus Perez VA, Alastalo TP, Alvira CM, Guignabert C, Bekker JM, Schellong S, Urashima T, Wang L, Morrell NW, et al. An antiproliferative BMP-2/PPARgamma/apoE axis in human and murine SMCs and its role in pulmonary hypertension. J Clin Invest. 2008;118:1846–1857. [PubMed: 18382765]
17. Spiekerkoetter E, Guignabert C, de Jesus Perez V, Alastalo TP, Powers JM, Wang L, Lawrie A, Ambartsumian N, Schmidt AM, Berryman M, et al. S100A4 and bone morphogenetic protein-2 codependently induce vascular smooth muscle cell migration via phospho-extracellular signal-regulated kinase and chloride intracellular channel 4. Circ Res. 2009;105:639–647. [PubMed: 19713532]
18. Perez VA, Ali Z, Alastalo TP, Ikeno F, Sawada H, Lai YJ, Kleisli T, Spiekerkoetter E, Qu X, Rubinos LH, et al. BMP promotes motility and represses growth of smooth muscle cells by activation of tandem Wnt pathways. J Cell Biol. 2011;192:171–188. doi: jcb.201008060 [pii] 10.1083/jcb.201008060 [PubMed: 21220513]
19. Yang X, Long L, Southwood M, Rudarakanchana N, Upton PD, Jeffery TK, Atkinson C, Chen H, Trembath RC, Morrell NW. Dysfunctional Smad signaling contributes to abnormal smooth muscle cell proliferation in familial pulmonary arterial hypertension. Circ Res. 2005;96:1053–1063. [PubMed: 15845886]
20. Tada Y, Majka S, Carr M, Harral J, Crona D, Kuriyama T, West J. Molecular effects of loss of BMPR2 signaling in smooth muscle in a transgenic mouse model of PAH. Am J Physiol Lung Cell Mol Physiol. 2007;292:L1556–1563. [PubMed: 17369292]
21. Yao C, Yu J, Taylor L, Polgar P, McComb ME, Costello CE. Protein Expression by Human Pulmonary Artery Smooth Muscle Cells Containing a BMPR2 Mutation and the Action of ET-1 as Determined by Proteomic Mass Spectrometry. Int J Mass Spectrom. 2015;378:347–359. doi: 10.1016/j.ijms.2014.10.006 [PubMed: 25866469]
22. Beppu H, Malhotra R, Beppu Y, Lepore JJ, Parmacek MS, Bloch KD. BMP type II receptor regulates positioning of outflow tract and remodeling of atrioventricular cushion during cardiogenesis. Dev Biol. 2009;331:167–175. doi: 10.1016/j.ydbio.2009.04.032 [PubMed: 19409885]
23. DeWire SM, Ahn S, Lefkowitz RJ, Shenoy SK. Beta-arrestins and cell signaling. Annu Rev Physiol. 2007;69:483–510. doi: 10.1146/annurev.physiol.69.022405.154749 [PubMed: 17305471]
24. Kim J, Zhang L, Peppel K, Wu JH, Zidar DA, Brian L, DeWire SM, Exum ST, Lefkowitz RJ, Freedman NJ. Beta-arrestins regulate atherosclerosis and neointimal hyperplasia by controlling smooth muscle cell proliferation and migration. Circ Res. 2008;103:70–79. doi: 10.1161/CIRCRESAHA.108.172338 [PubMed: 18519945]
25. Bonnans C, Flaceliere M, Grillet F, Dantec C, Desvignes JP, Pannequin J, Severac D, Dubois E, Bibeau F, Escriou V, et al. Essential requirement for beta-arrestin2 in mouse intestinal tumors with elevated Wnt signaling. Proc Natl Acad Sci U S A. 2012;109:3047–3052. doi: 10.1073/pnas.1109457109 [PubMed: 22315403]
26. Kovacs JJ, Hara MR, Davenport CL, Kim J, Lefkowitz RJ. Arrestin development: emerging roles for beta-arrestins in developmental signaling pathways. Dev Cell. 2009;17:443–458. doi: 10.1016/j.devcel.2009.09.011 [PubMed: 19853559]
27. Jilwan FN, Escourrou P, Garcia G, Jais X, Humbert M, Roisman G. High occurrence of hypoxemic sleep respiratory disorders in precapillary pulmonary hypertension and mechanisms. Chest. 2013;143:47–55. doi: 10.1378/chest.11-3124 [PubMed: 22878784]

28. Kiermayer C, Conrad M, Schneider M, Schmidt J, Brielmeier M. Optimization of spatiotemporal gene inactivation in mouse heart by oral application of tamoxifen citrate. Genesis. 2007;45:11–16. doi: 10.1002/dvg.20244 [PubMed: 17216603]
29. Regan JA, Mauro AG, Carbone S, Marchetti C, Gill R, Mezzaroma E, Valle Raleigh J, Salloum FN, Van Tassell BW, Abbate A, et al. A mouse model of heart failure with preserved ejection fraction due to chronic infusion of a low subpressor dose of angiotensin II. Am J Physiol Heart Circ Physiol. 2015;309:H771–778. doi: 10.1152/ajpheart.00282.2015 [PubMed: 26188021]
30. Chen M, Lichtler AC, Sheu TJ, Xie C, Zhang X, O'Keefe RJ, Chen D. Generation of a transgenic mouse model with chondrocyte-specific and tamoxifen-inducible expression of Cre recombinase. Genesis. 2007;45:44–50. doi: 10.1002/dvg.20261 [PubMed: 17211877]
31. Zhang W, Du L, Gunst SJ. The effects of the small GTPase RhoA on the muscarinic contraction of airway smooth muscle result from its role in regulating actin polymerization. Am J Physiol Cell Physiol. 2010;299:C298–306. doi: 10.1152/ajpcell.00118.2010 [PubMed: 20445174]
32. Rabinovitch M, Gamble WJ, Miettinen OS, Reid L. Age and sex influence on pulmonary hypertension of chronic hypoxia on recovery. Am J Physiol. 1981;240:H62–H72. [PubMed: 6450541]
33. Foster GE, Hanly PJ, Ahmed SB, Beaudin AE, Pialoux V, Poulin MJ. Intermittent hypoxia increases arterial blood pressure in humans through a Renin-Angiotensin system-dependent mechanism. Hypertension. 2010;56:369–377. doi: 10.1161/HYPERTENSIONAHA.110.152108 [PubMed: 20625082]
34. Lagna G, Ku MM, Nguyen PH, Neuman NA, Davis BN, Hata A. Control of phenotypic plasticity of smooth muscle cells by bone morphogenetic protein signaling through the myocardin-related transcription factors. J Biol Chem. 2007;282:37244–37255. doi: 10.1074/jbc.M708137200 [PubMed: 17947237]
35. Tsaousi A, Williams H, Lyon CA, Taylor V, Swain A, Johnson JL, George SJ. Wnt4/beta-catenin signaling induces VSMC proliferation and is associated with intimal thickening. Circ Res. 2011;108:427–436. doi: 10.1161/CIRCRESAHA.110.233999 [PubMed: 21193738]
36. Nagaoka T, Gebb SA, Karoor V, Homma N, Morris KG, McMurtry IF, Oka M. Involvement of RhoA/Rho kinase signaling in pulmonary hypertension of the fawn-hooded rat. J Appl Physiol (1985). 2006;100:996–1002. doi: 10.1152/japplphysiol.01028.2005 [PubMed: 16322374]
37. Rolfe BE, Worth NF, World CJ, Campbell JH, Campbell GR. Rho and vascular disease. Atherosclerosis. 2005;183:1–16. doi: 10.1016/j.atherosclerosis.2005.04.023 [PubMed: 15982657]
38. Sedzinski J, Hannezo E, Tu F, Biro M, Wallingford JB. RhoA regulates actin network dynamics during apical surface emergence in multiciliated epithelial cells. J Cell Sci. 2017;130:420–428. doi: 10.1242/jcs.194704 [PubMed: 28089989]
39. Bryja V, Gradl D, Schambony A, Arenas E, Schulte G. Beta-arrestin is a necessary component of Wnt/beta-catenin signaling in vitro and in vivo. Proc Natl Acad Sci U S A. 2007;104:6690–6695. doi: 10.1073/pnas.0611356104 [PubMed: 17426148]
40. Altomare DA, Zhang L, Deng J, Di Cristofano A, Klein-Szanto AJ, Kumar R, Testa JR. GSK690693 delays tumor onset and progression in genetically defined mouse models expressing activated Akt. Clin Cancer Res. 2010;16:486–496. doi: 10.1158/1078-0432.CCR-09-1026 [PubMed: 20075391]
41. Kumar S, Jiang MS, Adams JL, Lee JC. Pyridinylimidazole compound SB 203580 inhibits the activity but not the activation of p38 mitogen-activated protein kinase. Biochem Biophys Res Commun. 1999;263:825–831. doi: 10.1006/bbrc.1999.1454 [PubMed: 10512765]
42. Tapon N, Hall A. Rho, Rac and Cdc42 GTPases regulate the organization of the actin cytoskeleton. Curr Opin Cell Biol. 1997;9:86–92. doi: 10.1016/s0955-0674(97)80156-1 [PubMed: 9013670]
43. Thompson O, Moghraby JS, Ayscough KR, Winder SJ. Depletion of the actin bundling protein SM22/transgelin increases actin dynamics and enhances the tumourigenic phenotypes of cells. BMC Cell Biol. 2012;13:1. doi: 10.1186/1471-2121-13-1 [PubMed: 22257561]
44. Zhao YY, Zhao YD, Mirza MK, Huang JH, Potula HH, Vogel SM, Brovkovych V, Yuan JX, Wharton J, Malik AB. Persistent eNOS activation secondary to caveolin-1 deficiency induces pulmonary hypertension in mice and humans through PKG nitration. J Clin Invest. 2009;119:2009–2018. doi: 10.1172/JCI33338 [PubMed: 19487814]

45. El-Bizri N, Guignabert C, Wang L, Cheng A, Stankunas K, Chang CP, Mishina Y, Rabinovitch M. SM22{alpha}-targeted deletion of bone morphogenetic protein receptor 1A in mice impairs cardiac and vascular development, and influences organogenesis. Development. 2008;135:2981–2991. [PubMed: 18667463]
46. Delot EC, Bahamonde ME, Zhao M, Lyons KM. BMP signaling is required for septation of the outflow tract of the mammalian heart. Development. 2003;130:209–220. [PubMed: 12441304]
47. Guignabert C, Alvira CM, Alastalo TP, Sawada H, Hansmann G, Zhao M, Wang L, El-Bizri N, Rabinovitch M. Tie2-mediated loss of peroxisome proliferator-activated receptor-gamma in mice causes PDGF receptor-beta-dependent pulmonary arterial muscularization. Am J Physiol Lung Cell Mol Physiol. 2009;297:L1082–1090. [PubMed: 19801450]
48. Riascos-Bernal DF, Chinnasamy P, Gross JN, Almonte V, Egaña-Gorroño L, Parikh D, Jayakumar S, Guo L, Sibinga NES. Inhibition of Smooth Muscle β-Catenin Hinders Neointima Formation After Vascular Injury. Arterioscler Thromb Vasc Biol. 2017;37:879–888. doi: 10.1161/atvbaha.116.308643 [PubMed: 28302627]
49. Ma Z, Yu YR, Badea CT, Kovacs JJ, Xiong X, Comhair S, Piantadosi CA, Rajagopal S. Vascular Endothelial Growth Factor Receptor 3 Regulates Endothelial Function Through beta-Arrestin 1. Circulation. 2019;139:1629–1642. doi: 10.1161/CIRCULATIONAHA.118.034961 [PubMed: 30586762]
50. Ahn S, Kim J, Hara MR, Ren XR, Lefkowitz RJ. {beta}-Arrestin-2 Mediates Anti-apoptotic Signaling through Regulation of BAD Phosphorylation. J Biol Chem. 2009;284:8855–8865. doi: 10.1074/jbc.M808463200 [PubMed: 19171933]
51. Soh UJ, Trejo J. Activated protein C promotes protease-activated receptor-1 cytoprotective signaling through beta-arrestin and dishevelled-2 scaffolds. Proc Natl Acad Sci U S A. 2011;108:E1372–1380. doi: 10.1073/pnas.1112482108 [PubMed: 22106258]
52. Cleghorn WM, Bulus N, Kook S, Gurevich VV, Zent R, Gurevich EV. Non-visual arrestins regulate the focal adhesion formation via small GTPases RhoA and Rac1 independently of GPCRs. Cell Signal. 2018;42:259–269. doi: 10.1016/j.cellsig.2017.11.003 [PubMed: 29133163]
53. Alexander MR, Owens GK. Epigenetic control of smooth muscle cell differentiation and phenotypic switching in vascular development and disease. Annu Rev Physiol. 2012;74:13–40. doi: 10.1146/annurev-physiol-012110-142315 [PubMed: 22017177]
54. Tsai MC, Chen L, Zhou J, Tang Z, Hsu TF, Wang Y, Shih YT, Peng HH, Wang N, Guan Y, et al. Shear stress induces synthetic-to-contractile phenotypic modulation in smooth muscle cells via peroxisome proliferator-activated receptor alpha/delta activations by prostacyclin released by sheared endothelial cells. Circ Res. 2009;105:471–480. doi: 10.1161/CIRCRESAHA.109.193656 [PubMed: 19628794]
55. Zhang S, Fantozzi I, Tigno DD, Yi ES, Platoshyn O, Thistlethwaite PA, Kriett JM, Yung G, Rubin LJ, Yuan JX. Bone morphogenetic proteins induce apoptosis in human pulmonary vascular smooth muscle cells. Am J Physiol Lung Cell Mol Physiol. 2003;285:L740–754. doi: 10.1152/ajplung.00284.2002 [PubMed: 12740218]
56. Stypmann J, Engelen MA, Troatz C, Rothenburger M, Eckardt L, Tiemann K. Echocardiographic assessment of global left ventricular function in mice. Lab Anim. 2009;43:127–137. doi: 10.1258/la.2007.06001e [PubMed: 19237453]
57. Matthews VB, Rudnicka C, Schlaich MP. A cautionary note for researchers treating mice with the neurotransmitter norepinephrine. Biochem Biophys Rep. 2018;15:103–106. doi: 10.1016/j.bbrep.2018.08.003 [PubMed: 30148215]

Novelty and Significance

What is known?

- Mutations in bone morphogenetic protein receptor, type 2 (*BMPR2*) are associated with familial and sporadic pulmonary arterial hypertension (PAH) and reduced BMPR2 is associated with all forms of PAH.
- The functional and molecular link between loss of BMPR2 in pulmonary arterial smooth muscle cells (PASMC) and PAH pathogenesis warrants further investigation, as most investigations focus on the role of BMPR2 in PA endothelial cells.

What new information does this article contribute?

- We show that loss of BMPR2 causes impaired contractility and heightened proliferation of PASMC and contributes to the development of PAH.
- The hyperproliferative and hypo-contractile phenotype of PASMC with loss of BMPR2 results from elevated pERK1/2-pP38-pSMAD2/3-mediated increase in β-Arrestin2 (ARRB2), a scaffolding protein and consequent increase in pAKT-mediated nuclear translocation of active β-Catenin (CTNNB1), a transcriptional co-activator of genes important in proliferation. At the same time, increased ARRB2 results in a reduction in RHOA/RAC1, as well as TAGLN and filament actin, negatively impacting the contractile apparatus.
- ARRB2 and nuclear CTNNB1 are elevated in PASMC of PAH patients with a *BMPR2* mutation, compared to PASMC of healthy controls.

Our findings indicate that compromise in *BMPR2* function in PASMC severely impacts the contractile and well-differentiated phenotype, by a mechanism in which activation of the TGFβ signaling pathway elevates ARRB2, a scaffolding protein necessary for pAKT mediated translocation of CTNNB1 a transcriptional co-activator of proliferation genes. Targeting elevated ARRB2 in could prevent the pathological phenotype of PASMC that underlies the progression of PAH.

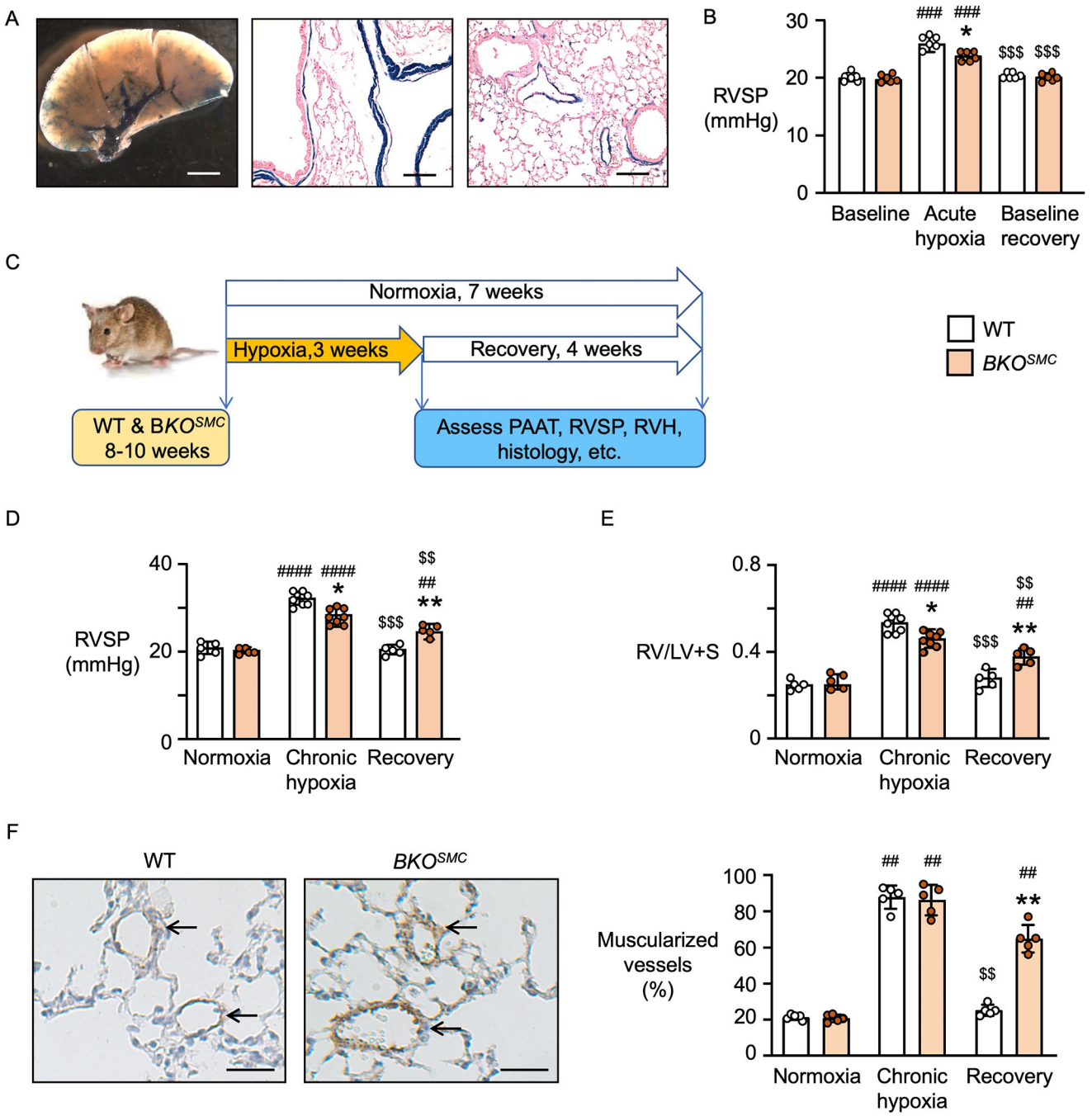

Figure 1. *Tagln-Cre/R26R/Bmpr2*−/− (*BKO*^{SMC}) mice exhibit reduced vasoreactivity and persistent pulmonary hypertension (PH) following recovery from chronic hypoxia.

BKO^{SMC} and wild type (WT) littermate were exposed to chronic or acute hypoxia, and compared to mice housed under normoxia (room air). **(A)** Representative mouse left lung with LacZ staining in pulmonary arteries (scale bar: 3 mm) and H&E stained lung sections (7 μm thick, scale bar: 100 μm). **(B)** Pulmonary vascular reactivity: Continuous RVSP measurements were obtained in ventilated, anesthetized mice under the following sequence: 40% O_2 for 5 minutes (baseline), followed by 10% O_2 for 15 minutes (acute hypoxia),

and 15 minutes in 40% O_2 (baseline recovery). **(C-F)** Chronic hypoxia: Mice were exposed to three weeks of hypoxia (10% O_2) followed by four weeks recovery in normoxia, or followed for seven weeks in normoxia. (**C**) Experimental design. **(D)** Right ventricular systolic pressure (RVSP). **(E)** Right ventricular (RV) hypertrophy, weight ratio of RV vs. LV+Septum. **(F)** Muscularity of distal arteries at alveolar wall and duct level (Images on the left are from the recovery groups, scale bar: 25 μm). Data represent mean±SEM, n=5–8 mice per group, $^{*}P<0.05$, $^{**}P<0.01$, $^{****}P<0.0001$ *BKO* vs. WT, under the same conditions; $^{\#\#}P<0.01$, $^{\#\#\#}P<0.001$, $^{\#\#\#\#}P<0.0001$ vs. room air or baseline, same genotype; and $^{\$\$}P<0.01$, $^{\$\$\$}P<0.001$, $^{\$\$\$\$}P<0.0001$, recovery vs. hypoxia or acute hypoxia, same genotype. Analyses performed by unpaired two-way ANOVA, and adjusted for multiple comparisons using Tukey's post hoc test in (A-E), and by non-parametric Kruskal-Wallis one-way ANOVA, adjusted for multiple comparisons using the Dunn's post hoc test in (F).

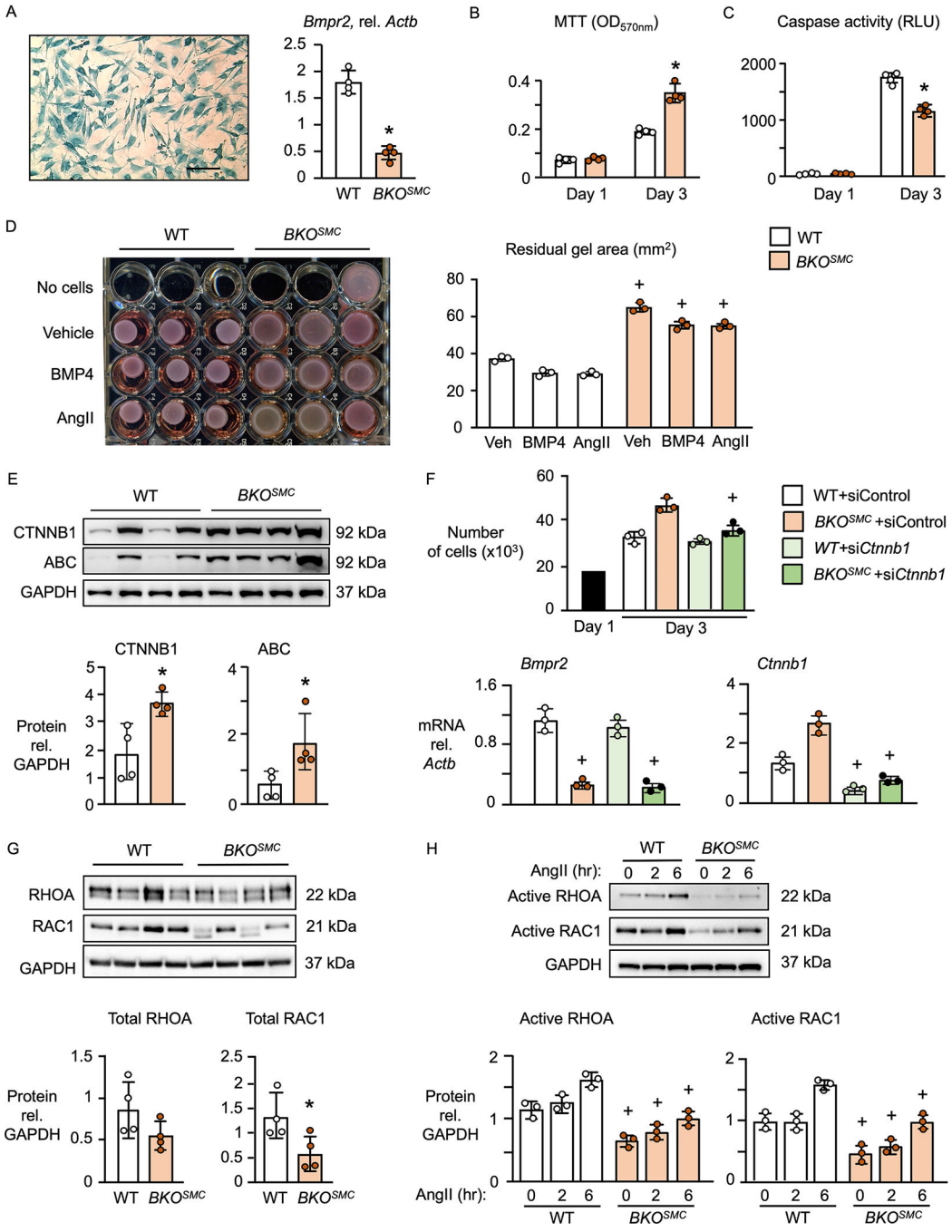

Figure 2: Heightened proliferation and impaired contractility in *Tagln-Cre/R26R/Bmpr2*$^{-/-}$ (*BKO*^{SMC}) PASMC related to elevated β-Catenin (CTNNB1) and decreased RHOA and RAC1.

Murine (m) PASMC were isolated from large PA of *BKO*^{SMC} and littermate controls. Each data point is a biological replicate, representing mPASMC isolated by combining 2–3 PAs (see Methods). **(A)** Representative image of LacZ stained mPASMC in culture (Scale bar, 50 μm) with quantitative real time PCR of mPASMC on the right, attesting to the knockdown *Bmpr2* in the mPASMC. **(B)** Proliferation, assessed by MTT assay in 96-well plates with 1,000 mPASMC seeded per well. **(C)** Survival, assessed by Caspase 3/7 Assay in

96-well plates with 20,000 mPASMC seeded per well following serum withdrawal. **(D)** Gel contractility assay of PASMC from *BKO*^{SMC} vs. WT mice. mPASMC were evenly mixed with collagen gel and seeded on 48-well plates (3×10^5 cells per 250 μL of gel per well). The embedded cells were treated with vehicle (0.1% BSA in PBS), BMP4 (10 ng/mL) or Angiotensin II (AngII, 4 μM) for 72 hours. The residual gel area was analyzed by ImageJ. Wells with the gel without embedded cells served as a negative control. **(E)** Representative immunoblot of CTNNB1 and active β-Catenin (ABC) in WT or *BKO*^{SMC} mPASMC, with densitometric analysis relative to ACTB as loading control. **(F)** Proliferation assessed by cell counts. On day 1, 20,000 mPASMC were seeded per well in 6-well plates, comparing mPASMC from *BKO*^{SMC} and WT mice where *Ctnnb1* was reduced by siRNA, vs. treatment with non-targeting siRNA (siControl). Quantitative real time PCR below, attesting to the knock-down of *Bmpr2* and *Ctnnb1* in the mPASMC. **(G)** Representative immunoblot of total RHOA and RAC1 in mPASMC of *BKO*^{SMC} vs. WT mice, with densitometric analysis relative to GAPDH as loading-control. **(H)** Representative immunoblot of active RHOA and RAC1 in mPASMC of *BKO*^{SMC} vs. WT mice, at baseline (0 hour) and in response to AngII (4 μM) stimulation for 2 or 6 hours, with densitometric analysis relative to GAPDH as loading control. In (E, G and H), data were normalized to the lane on the left.
Data represent mean±SEM. Data were analyzed by non-parametric Kolmogorov-Smirnov t-test. In (A, B, C, E, G), n=4 biological replicates; **P*<0.05 vs. WT. In (D and H), n=3 biological replicates; + denotes comparisons vs. WT at the same time point or treatment condition, where the minimum achievable *P*-value for n=3 was reached by the non-parametric t-test. In (F), n=3 biological replicates; + denotes comparison of si*Ctnnb1* in the same genotype (cell number and *Ctnnb1* mRNA), or confirms *Bmpr2* knockdown.

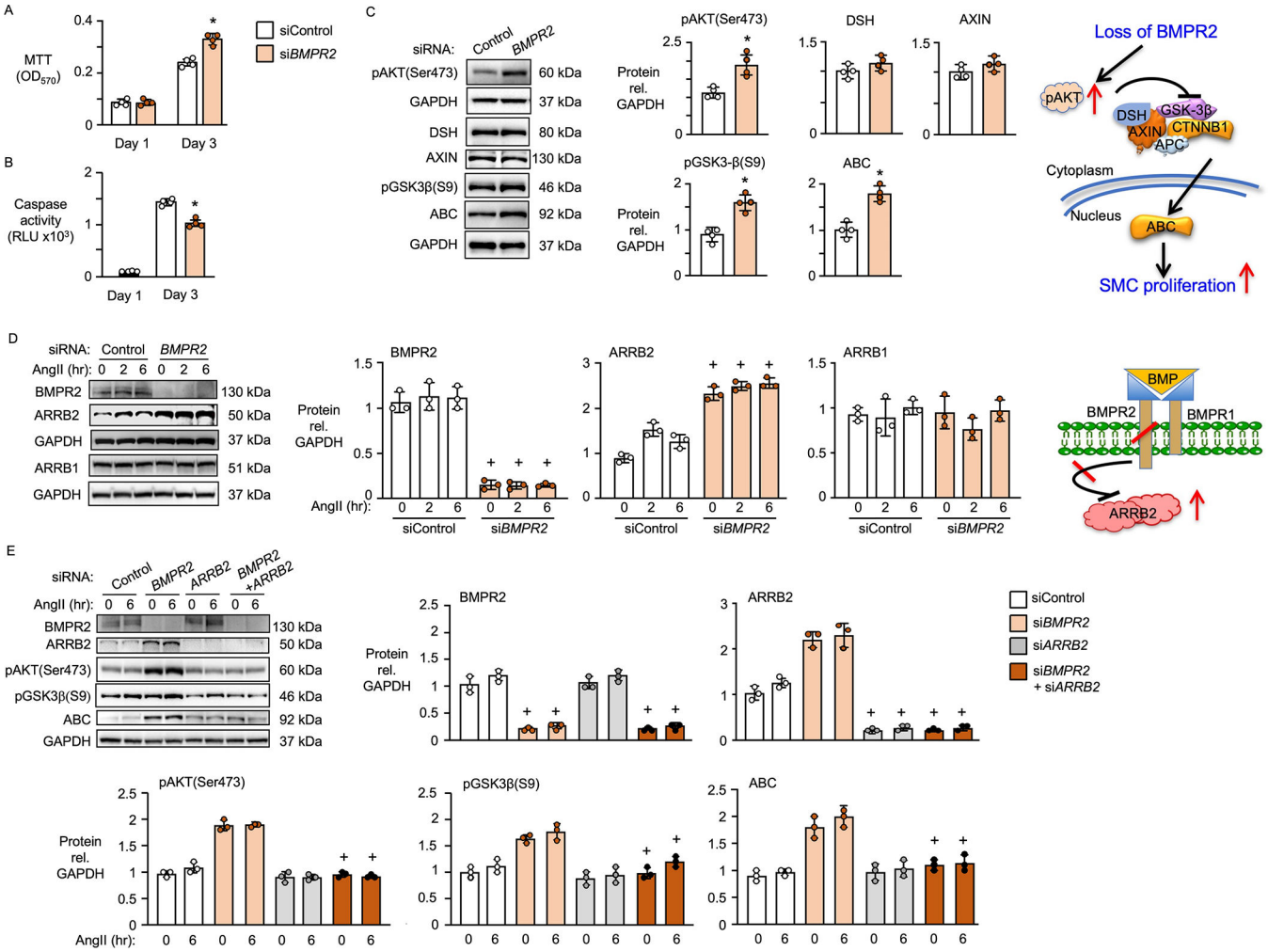

Figure 3: Loss of BMPR2 in human PASMC increases proliferation and survival related to β-Arrestin 2 (ARRB2) dependent activation of pAKT and ABC.

Human PASMC isolated from small pulmonary arteries (PA) of unused donor lungs were cultured as described in Methods and transfected with siRNA targeting *BMPR2* (*siRMPR2*) or non-targeting siRNA (siControl). **(A)** Proliferation, assessed by MTT assay in 96-well plates with 1,000 PASMCs seeded per well. **(B)** Survival, assessed by Caspase 3/7 Assay following serum withdrawal. On day 1, in 96-well plates, 20,000 PASMCs were seeded per well. **(C)** Representative immunoblots of pAKT(Ser473), DSH, AXIN, inactive pGSK3-β [pGSK3-β(S9)] and ABC in PASMC, with densitometric analysis, and schema of the signaling pathway on the right. **(D)** Representative immunoblot of BMPR2, ARRB2 and ARRB1 in PASMC in response to AngII (4 μM) stimulation for 2 or 6 hours, with densitometric analysis, and schema of the signaling pathway on the right. **(E)** *BMPR2*, *ARRB2* or both genes were reduced in PASMC by siRNA, compared with siControl. BMPR2, ARRB2, pAKT(Ser473), pGSK3-β(S9), and ABC were analyzed by western blot following stimulation with AngII (4 μM) for 6 hours. In (C, D and E), Densitometric analysis relative to GAPDH as loading control, normalized to the lane on the left. Data represent mean±SEM. Data were analyzed by non-parametric Kolmogorov-Smirnov t-test. In (A-C) n=4 Donors; **P*<0.05, vs. siControl under the same conditions. In (D, E),

n=3; + denotes the minimum achievable *P*-value for n=3 was reached by the non-parametric t-test comparing si*BMPR2* vs. siControl under the same conditions in (D), and si*ARRB2* in the same genotype at the same time point, or confirms reduced BMPR2 with siRNA in (E).

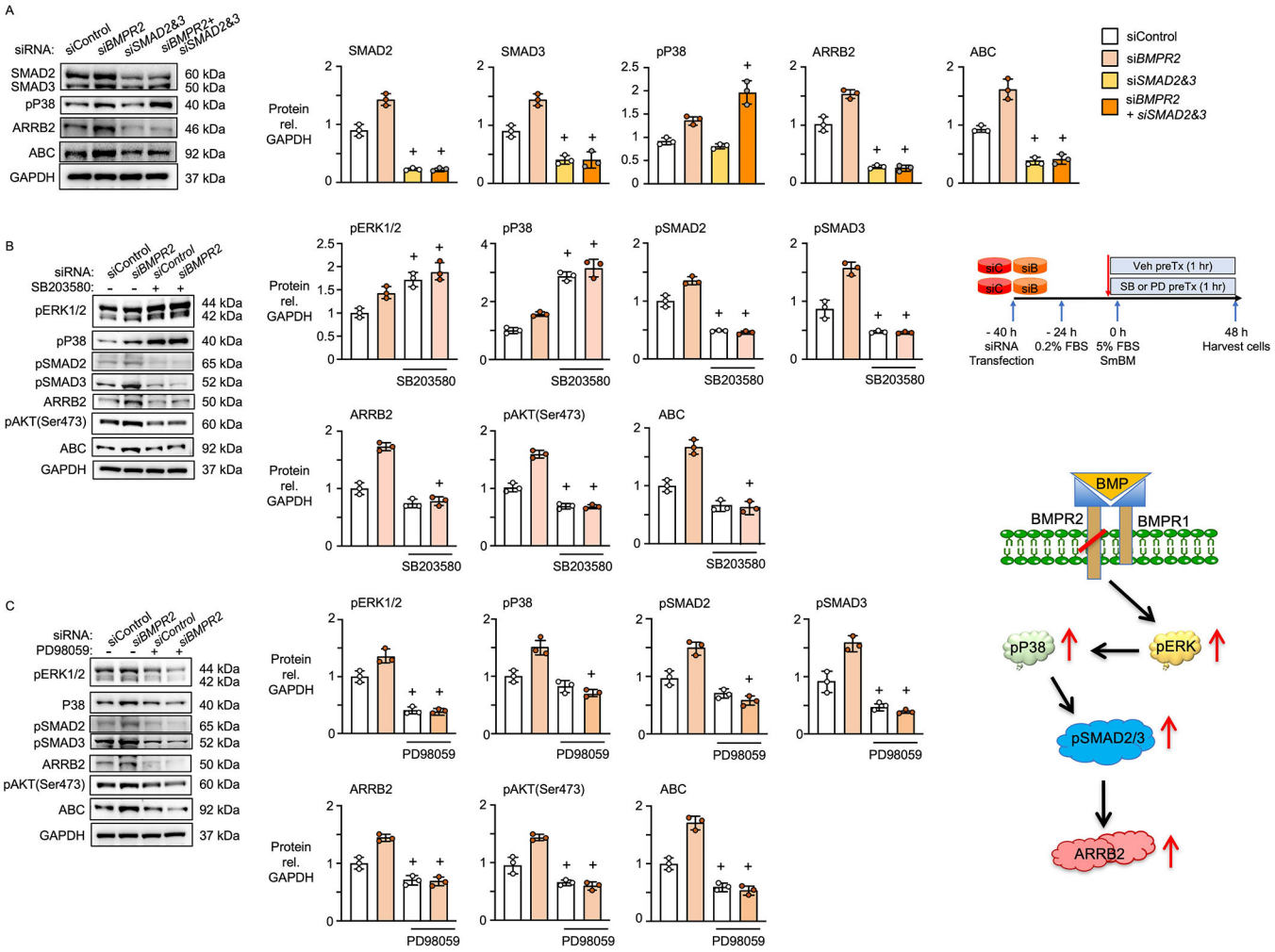

Figure 4: Loss of BMPR2 in human PASMC increases pERK, pP38 and pSMAD 2&3, associated with an increase in ARRB2 and ABC.

Human PASMC isolated from small PA of unused donor lungs were cultured as described in Methods and transfected with siRNA targeting *BMPR2* (si*RMPR2*) or with non-targeting siRNA (siControl). **(A)** PASMC transfected with siRNA targeting *BMPR2* (si*RMPR2*), *SMAD2&3* (si*SMAD2* and si*SMAD3*), or both, compared with non-targeting siRNA (siControl). Representative immunoblots of SMAD2&3, pP38(MAPK), ARRB2 and ABC in PASMC, with densitometric analysis. **(B)** and **(C)** si*BMPR2* and siControl transfected PASMC were pretreated with **(B)** pP38(MAPK) inhibitor, SB203580 (10 μM) or with **(C)** pERK1/2 inhibitor, PD98059 (20 μM) for 1 hour prior to culture for 48 hours and compared with the vehicle groups. Representative immunoblots of pERK1/2, pP38(MAPK), pSMAD2&3, ARRB2, pAKT(Ser473) and ABC in PASMC, with densitometric analysis. On the right, experimental design and schema representing the pathway we propose based on this study. Data show protein relative to GAPDH as loading control, normalized to the lane on the left.

Data represent mean±SEM of n=3 Donors. Data were analyzed by non-parametric Kolmogorov-Smirnov t-test. + denotes comparisons where the minimum achievable *P*-value

for n=3 was reached, comparing the effect of si*SMAD2&3* or inhibitor treatment in siControl or in si*BMPR2*.

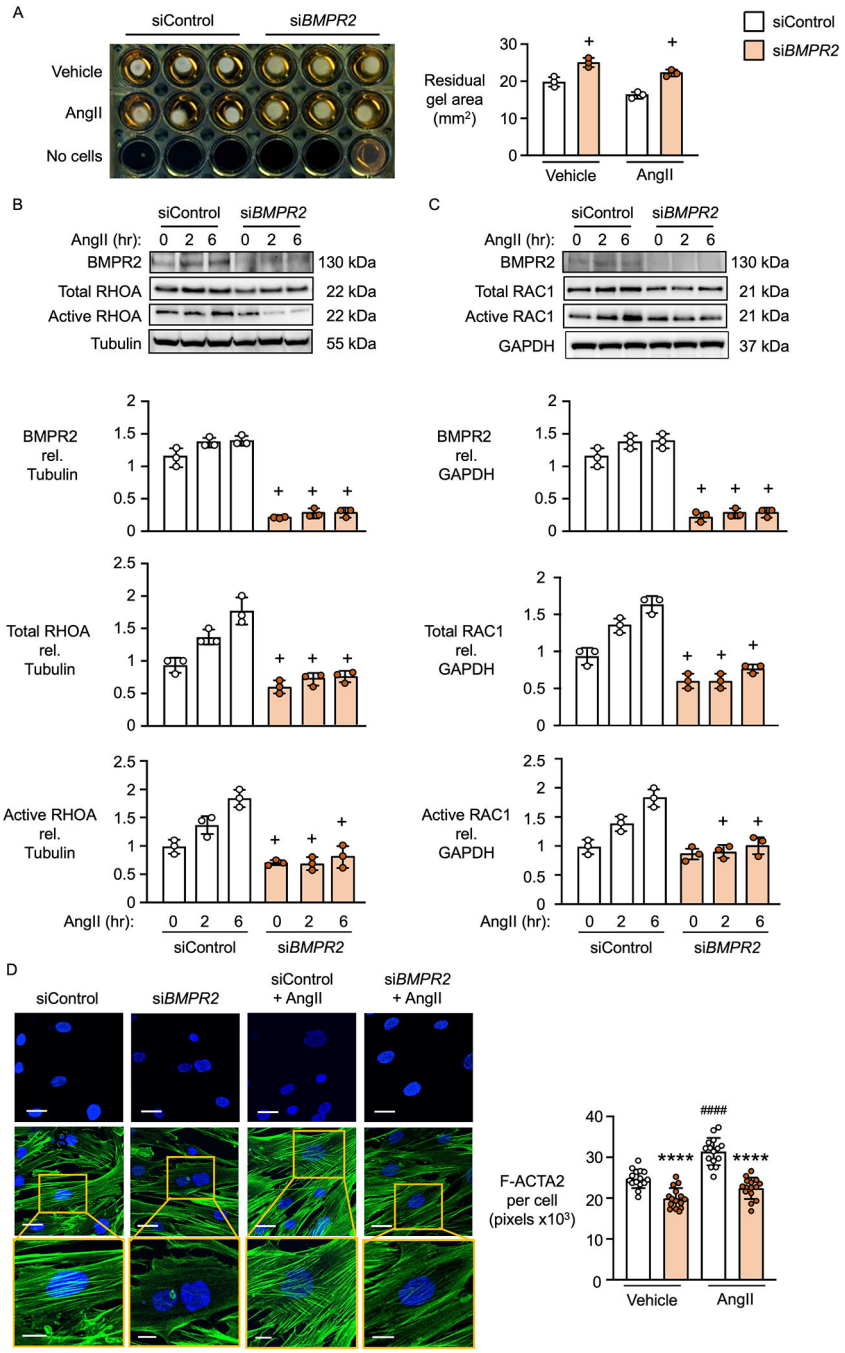

Figure 5: Human PASMC with loss of BMPR2 show reduced contractility, related to reduced RHOA and RAC1, and ACTA2 fibers (F-ACTA2).

Human PASMC were isolated from small PA of unused donor lungs, cultured as described under ‘Methods’, and transfected with siRNA targeting *BMPR2* (si*RMPR2*) or with non-targeting siRNA (siControl). **(A)** Gel contractility assay, as described for Figure 2D, following stimulation by Angiotensin II (AngII, 4 μM) or vehicle (PBS) for 72 hours. **(B, C)** PASMC were treated with AngII (4 μM) for 2 or 6 hours, compared with baseline (0 time). Representative immunoblot of BMPR2, total and active RHOA (in B), and BMPR2, total

and active RAC1 (in C), with densitometric analysis relative to GAPDH as loading control, normalized to the lane on the left. **(D)** Confocal microscopic images of PASMC following AngII (4 μM) or vehicle (PBS) stimulation for 6 hours, showing filament actin fibers probed by Phalloidin conjugates (green) and nuclei stained by DAPI (blue). Average F-ACTA2 per cell (total F-ACTA2 pixels divided by the number of nuclei in each field) was determined using Fuji ImageJ. Scale bar, 30 μm (top and middle rows); 15 μm for zoomed in images, bottom row.

Data represent mean±SEM. (A-C) n=3 Donors; + denotes comparisons vs. siControl under the same condition, where the minimum achievable *P*-value for n=3 was reached by non-parametric Kolmogorov-Smirnov t-test. (D) n=15 fields; ****$P<0.0001$ vs. siControl under the same condition, and $^{\#\#\#\#}P<0.05$, comparing the same genotype across conditions, by one way ANOVA adjusted for multiple comparisons using Tukey's post hoc test.

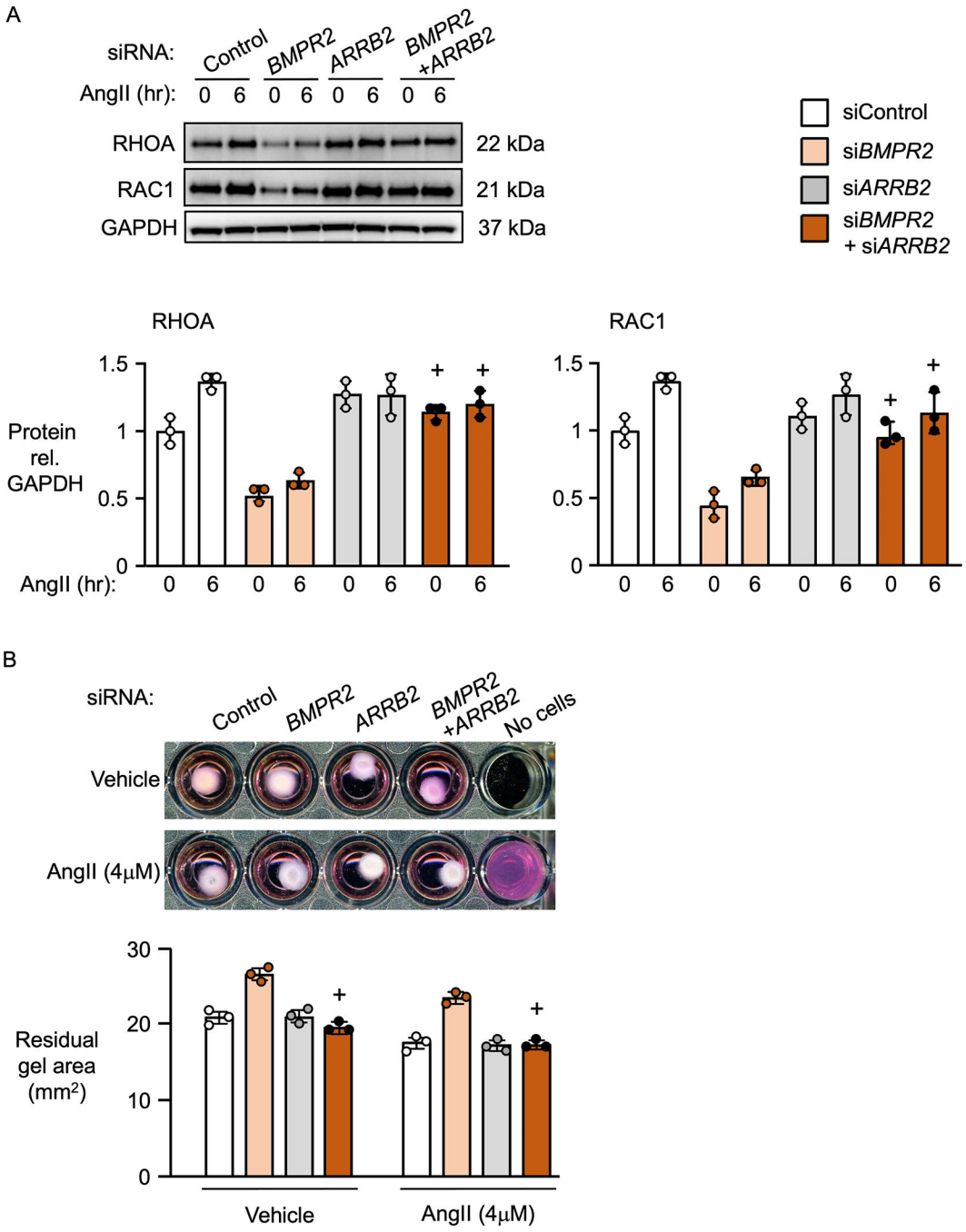

Figure 6: Reducing ARRB2 in PASMC with loss of BMPR2 restores normal levels of RHOA, RAC1 and contractility.

Human PASMC isolated from small pulmonary arteries of unused donor lungs were cultured as described under 'Methods', and transfected with siRNA targeting *BMPR2* (si*BMPR2*), *ARRB2* (si*ARRB2*), or both, vs. non-targeting siRNA (siControl). **(A)** Representative immunoblot of total RHOA and RAC1 in PASMC in response to AngII (4 μM) stimulation for 6 hours or at baseline (time 0), with densitometric analysis relative to GAPDH as loading control, normalized to the lane on the left. (Reduction of BMPR2 and ARRB2 by siRNA in

the same sample is shown in Figure 3E). **(B)** Gel contractility assay (representative image), as described in Figure 2D, in PASMC transfected with si*BMPR2,* si*ARRB2*, or both, vs. siControl transfected cells, in response to AngII (4 μM) or vehicle (0.1% BSA in PBS) stimulation for 72 hours.

Data represent mean±SEM of n=3 donors; + denotes comparisons where the minimum achievable *P*-value for n=3 was reached by non-parametric Kolmogorov-Smirnov t-test comparing the effect of si*ARRB2* in siControl or in si*BMPR2* at the same time point or treatment condition.

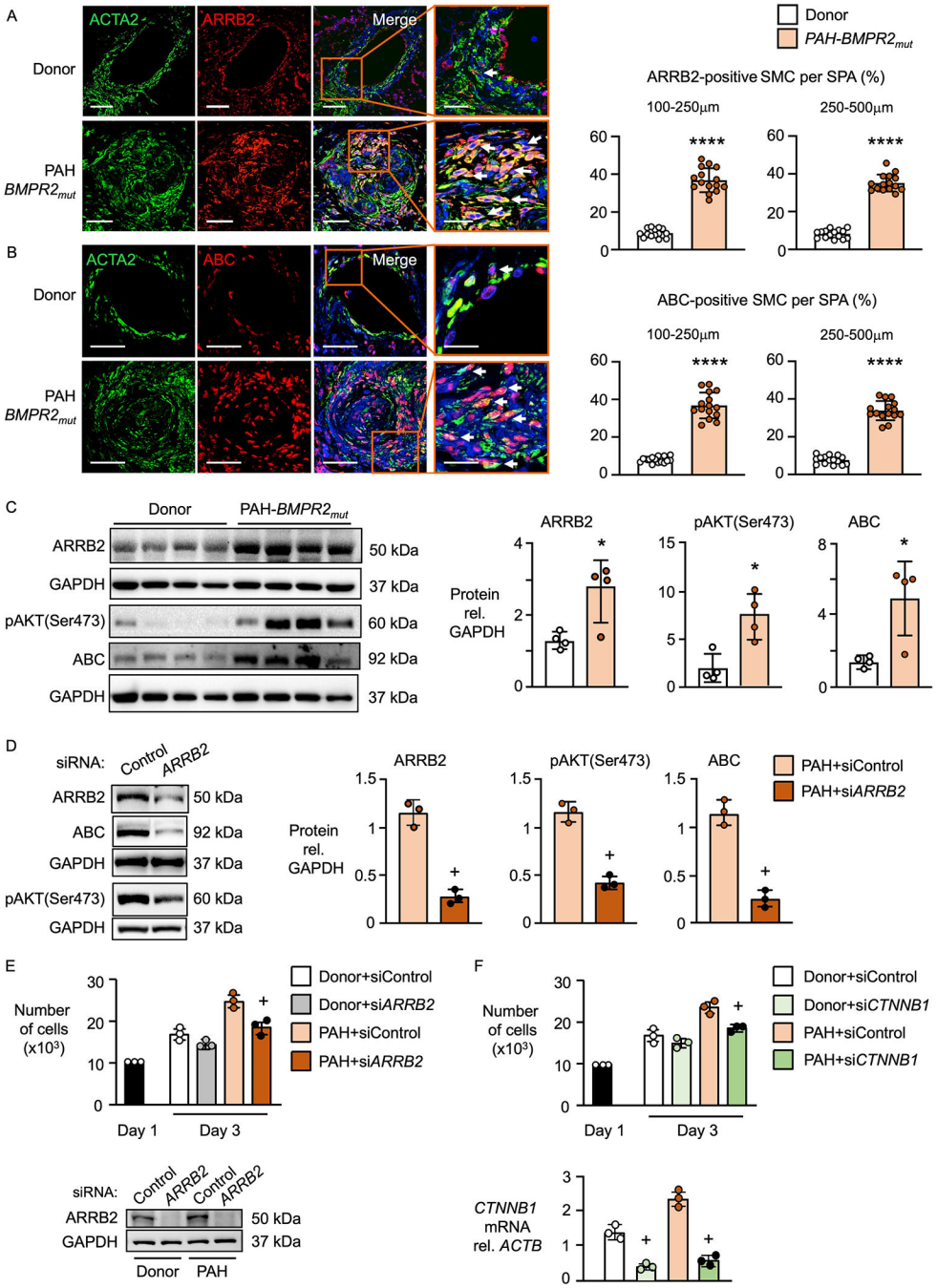

Figure 7: Increased proliferation and survival in PASMC of PAH patients with *BMPR2* mutation, related to activation of ARRB2-pAKT-ABC axis.

(A, B) Human lung tissue sections (7 μm thick) from PAH patients with a *BMPR2* mutation (PAH- $BMPR2_{mut}$), or from donor lungs (Donor), were probed with antibodies against ARRB2, ABC or ACTA2, and imaged by confocal microscopy. Terminal bronchiolus PA (SPA) at two levels, 100–250 μm and 250–500 μm were assessed from 3 Donors or PAH-mut patients and 5 random fields for each Donor or PAH patient. **(A, B)** Representative Immunofluorescent staining of ARRB2 or ABC (red), ACTA2 (green) and nuclei (DAPI,

blue). Arrows in zoomed images on the right point to PASMC with abundant ARRB2 in the cytoplasm (in A) and ABC in the nucleus (in B). Scale bars, 50 μm in the three left columns, 20 μm, right column. **(C-F)** PASMC were isolated from SPA of PAH-*BMPR2*$_{mut}$ patients, or from unused donor lungs. **(C)** Representative immunoblot of ARRB2, pAKT(Ser473) and ABC in PASMC, with densitometric analysis relative to GAPDH as loading control. **(D)** PASMC from PAH-*BMPR2*$_{mut}$ patients were transfected with siRNA targeting ARRB2 (si*ARRB2*) or with non-targeting siRNA (siControl), and ARRB2, pAKT(Ser473) and ABC evaluated by immunoblots. Representative blots are shown, with densitometric analysis relative to GAPDH as loading control. In (C, D), data was normalized to the lane on the left. **(E)** Proliferation, assessed by cell counts with 10,000 PASMCs seeded per well in 24-well plates at day 1, comparing PAH-*BMPR2*$_{mut}$ vs. Donor PASMC transfected with si*ARRB2* vs. siControl, and plated at the same initial density. Representative immunoblot below, attesting to the reduction of ARRB2 in the PASMC. **(F)** Proliferation, assessed by cell counts similar to (E), under the conditions of Figure 6E, comparing treatment by si*CTNNB1* vs. siControl. Quantitative real time PCR below, attesting to the reduction of *CTNNB1* in the PASMC.

Data represent mean±SEM. (A and B) n=15 fields, **** $P<0.0001$ vs. Donor by parametric t-test with Welch's correction. (C) n=4 PAH patients or donors; * $P<0.05$ vs. Donor PASMC by non-parametric Kolmogorov-Smirnov t-test. (D, E, F) n=3 PAH patients or Donors; + denotes comparisons where the minimum p value was achieved by the non-parametric test comparing si*ARRB2* vs. siControl in (D, E), or si*CTNNB1* vs. siControl in (F), in the Donor or PAH patient PASMC.

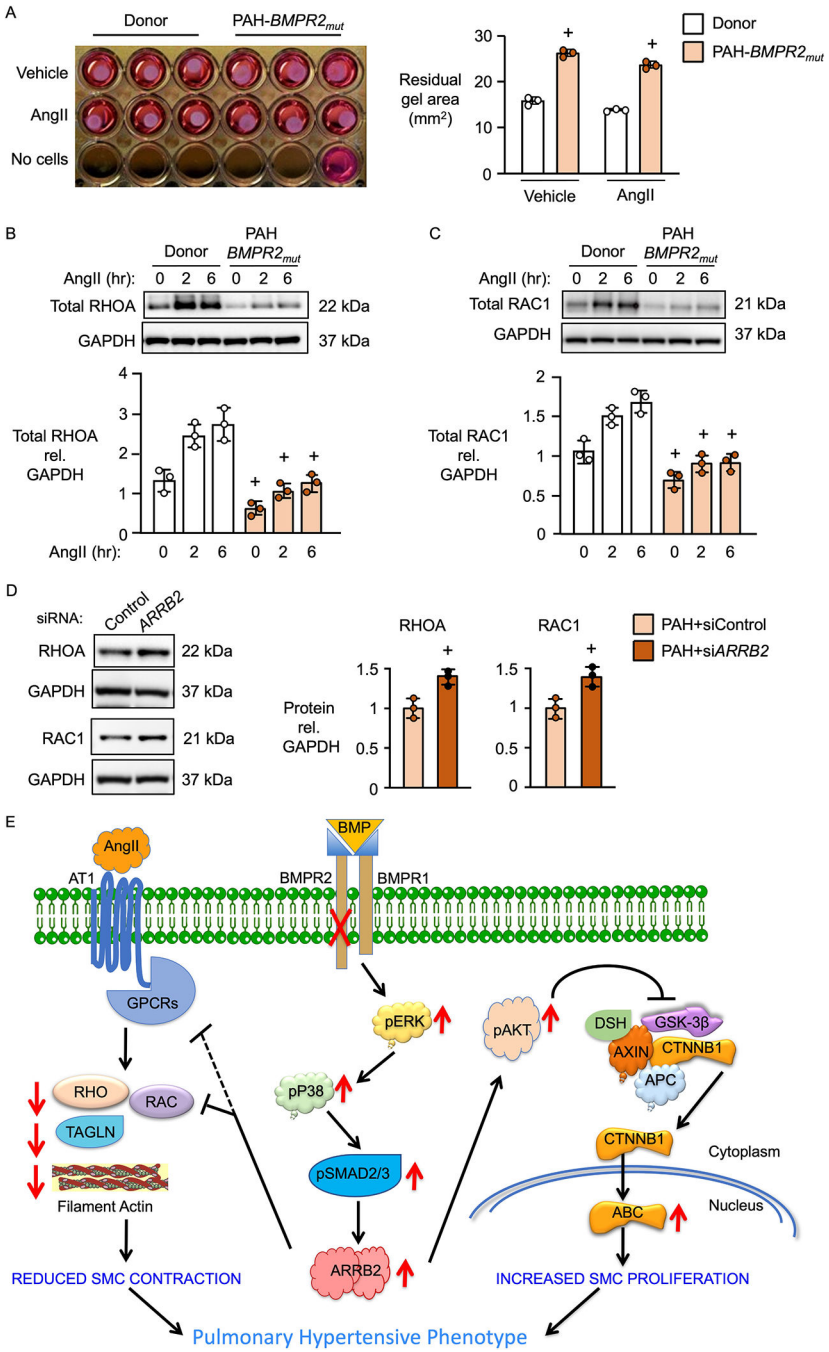

Figure 8: PASMC from PAH-*BMPR2*$_{mut}$ patients show reduced contractility, related to reduced RHOA and RAC1. Reducing ARRB2 restores RHOA and RAC1.

PASMC were isolated from small PAs of PAH-*BMPR2*$_{mut}$ or from unused donor lungs as controls (Donor). **(A)** Gel contractility assay, as described for Figure 2D, following AngII (4 μM) or vehicle stimulation. Residual gel area (mm^2) was analyzed by ImageJ. **(B, C)** Representative immunoblot of total RHOA (B) and total RAC1 (C), in response to AngII (4 μM) for 2 and 6 hours vs. time 0 (baseline), with densitometric analysis. **(D)** ARRB2 was reduced by siRNA targeting *ARRB2* (si*ARRB2*) vs. siControl in PASMC from PAH-

BMPR2$_{mut}$ as shown in Figure 7D. Representative immunoblots of ARRB2, RHOA and RAC1, with densitometric analysis. In (B, C, D), densitometric analysis is shown relative to GAPDH as loading control, normalized to the lane on the left.

Data represent mean±SEM of n=3 Donors or PAH patients; + denotes comparisons where the minimum achievable *P*-value for n=3 was reached by the non-parametric Kolmogorov-Smirnov t-test, comparing PAH-BMPR2$_{mut}$ vs. Donors under the same condition in (A-C), or si*ARRB2* vs. siControl in D.

(E) Model: Schematic diagram summarizing the findings. Reduced BMPR2 in SMC leads to pERK-pP38-pSMAD2/3 dependent increase in ARRB2. The increase in ARRB2 results in pAKT-GSK3β mediated activation of CTNNB1, leading to increased proliferation. Increased ARRB2 leads to reduced RHOA and RAC1, and actin stress fibers, resulting in impaired contractility. The dashed line indicates association per published reports[23].

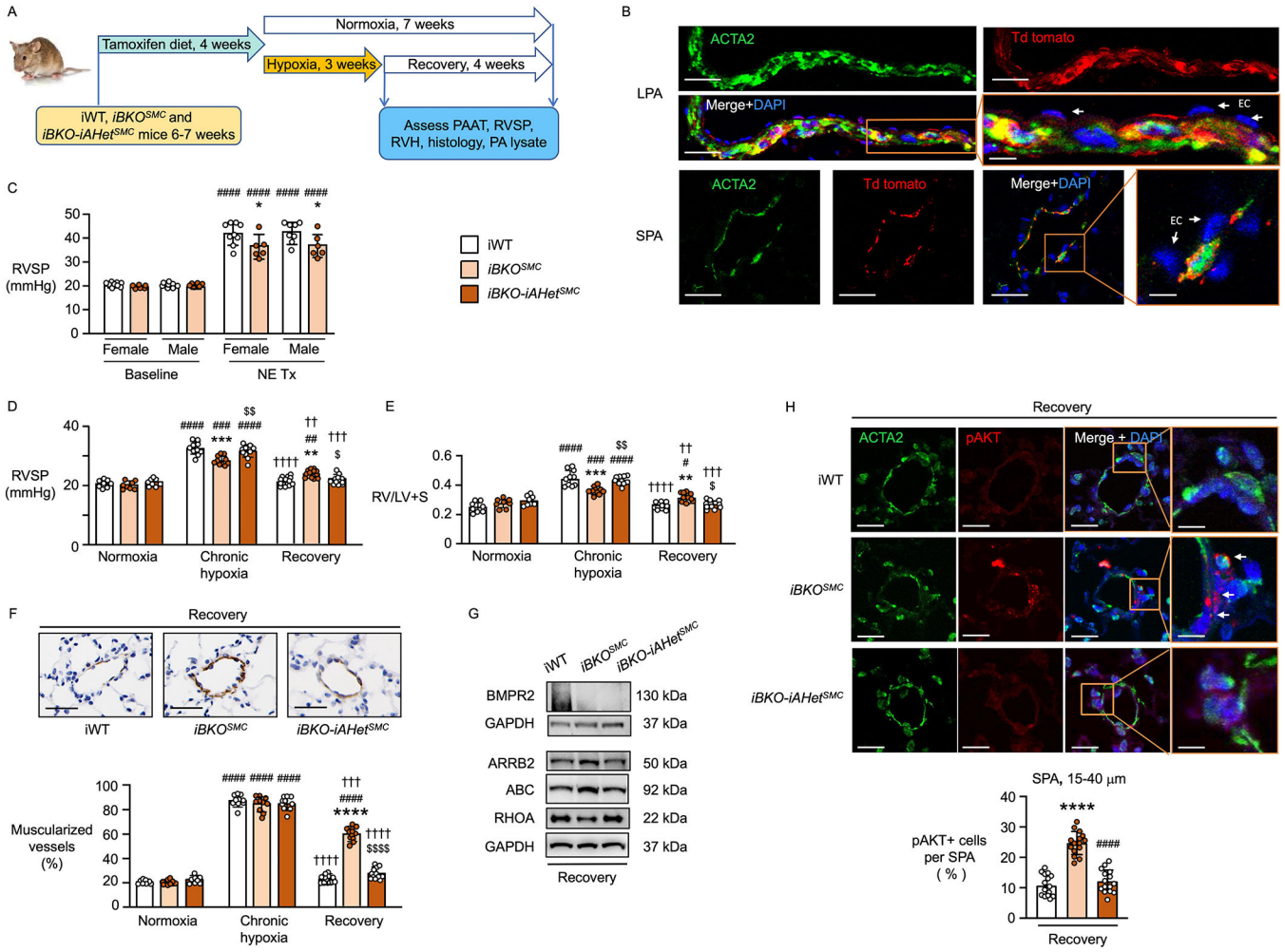

Figure 9: Reducing ARRB2 in *Acta2-CreER/Td/Bmpr2*$^{-/-}$ (*iKO*^{SMC}) mice prevents development of pulmonary hypertension.

(A) Experimental design: Mice with tamoxifen-inducible *Bmpr2* knock-out in SMC (*iBKO*^{SMC}), or *iBKO*^{SMC} mice with one *Arrb2* allele deleted (*Acta2-CreER/Td/Bmpr2*$^{-/-}$/*Arrb2*$^{-/+}$; (*iBKO-iAHet*^{SMC}), and controls (iWT) were exposed to chronic hypoxia as described in Figure 1C. **(B)** Representative Immunofluorescent staining of Td tomato (red), ACTA2 (green) and nuclei (DAPI, blue) from mouse lung sections (7 µm thick) obtained from *iBKO*^{SMC} mice. The ACTA2-CreER is selectively knocking out *Bmpr2* in SMC. No Td tomato expression in ECs (arrow). Scale bar: 25 µm; 5 µm in magnified panels. **(C)** Vasoreactivity assessment with Norepinephrine (NE): continuous RVSP measurement on *iBKO*^{SMC} vs. iWT (females and males) at baseline and NE treatment (Tx) (IV 20 µg/30 g BW in 1 min). **(D)** Right ventricular systolic pressure (RVSP) and **(E)** Right ventricular (RV) hypertrophy, weight ratio of RV vs. left ventricle and septum (RV/LV+S) of mice housed in room air, chronic hypoxia, and following recovery in room air. **(F)** Muscularity of distal arteries at alveolar wall and duct level. Images are from the recovery group (7 µm thick; scale bar: 25 µm). **(G)** Large PA (LPA) isolated from the recovery cohorts, iWT, *iBKO*^{SMC} and *iBKO-iAHet*^{SMC} mice. Lysates were prepared after removal of the EC and adventitial fibroblast layers. Representative immunoblot of BMPR2, ARRB2, ABC,

and RHOA, with GAPDH as loading control, confirming this regulatory pathway in the *iBKO*^{SMC} and *iBKO-iAHet*^{SMC} mice. Each lane represents combined LPA from four mice (n=4). **(H)** Representative Immunofluorescent staining of pAKT(Ser473) (red), ACTA2 (green) and nuclei (DAPI, blue) from mouse lung sections (7 μm thick) obtained from the recovery cohorts, iWT, *iBKO*^{SMC} and *iBKO-iAHet*^{SMC} (n=5 mice per group). Scale bars: 15μm; 4μm in magnified panels. Each point represents the average number of positive pAKT cells per SPA (15–40 μm) per field, from 3 random sections per mouse.
Data represent mean±SEM. (C) n=6 or n=9 (iWT females) and n=8 (iWT males); **P*<0.05 vs. iWT, under the same condition; $^{\#\#\#\#}P$<0.0001, vs. baseline, same genotype and same gender. (D, E, F) n=8, 10 or 12 mice (normoxia, hypoxia and recovery, respectively); ***P*<0.01, ****P*<0.001, *****P*<0.0001 vs. iWT under the same conditions; $^{\#}P$<0.05, $^{\#\#}P$<0.01, $^{\#\#\#}P$<0.001, $^{\#\#\#\#}P$<0.0001 vs. normoxia, same genotype; $^{\$}P$<0.05, $^{\$\$}P$<0.01, $^{\$\$\$\$}P$<0.0001 vs. *iBKO* under the same conditions; $^{\dagger\dagger}P$<0.01, $^{\dagger\dagger\dagger}P$<0.001, $^{\dagger\dagger\dagger\dagger}P$<0.001 vs. Hypoxia, same genotype. (C-F) Analyses performed by two-way ANOVA and Tukey's multiple comparisons test. (H) n=15 fields; ****<0.0001 vs. iWT, $^{\#\#\#\#}P$<0.0001, vs. *iBKO*^{SMC} under same condition, by one-way ANOVA with adjustment for multiple comparisons using Tukey's post hoc test.